Cerebral Cortex, December 2018;28: 4454–4471

doi: 10.1093/cercor/bhy258
Advance Access Publication Date: 11 October 2018
Original Article

ORIGINAL ARTICLE

Neural stem cell lineage-specific cannabinoid type-1 receptor regulates neurogenesis and plasticity in the adult mouse hippocampus

Tina Zimmermann[1], Mattia Maroso[2], Annika Beer[1], Sarah Baddenhausen[1], Susann Ludewig[3], Wenqiang Fan[1], Constance Vennin[1,4], Sebastian Loch[1], Benedikt Berninger[1,5], Clementine Hofmann[1], Martin Korte[3,6], Ivan Soltesz[2], Beat Lutz[1,4] and Julia Leschik[1]

[1]Institute of Physiological Chemistry, University Medical Center of the Johannes Gutenberg University Mainz, Germany, [2]Department of Neurosurgery, Stanford University, USA, [3]Zoological Institute, Division Cellular Neurobiology, TU Braunschweig, Germany, [4]German Resilience Center (DRZ), Mainz, [5]Institute of Psychiatry, Psychology & Neuroscience, Centre for Developmental Neurobiology and MRC Centre for Neurodevelopmental Disorders, King's College London, SE1 1 UL, UK and [6]Helmholtz Centre for Infection Research, Research group Neuroinflammation and Neurodegeneration, Braunschweig, Germany

Address correspondence to Julia Leschik, Institute of Physiological Chemistry, University Medical Center of the Johannes Gutenberg University, Duesbergweg 6, 55128 Mainz, Germany, Email: leschik@uni-mainz.de

Beat Lutz and Julia Leschik are shared senior authorship

Abstract

Neural stem cells (NSCs) in the adult mouse hippocampus occur in a specific neurogenic niche, where a multitude of extracellular signaling molecules converges to regulate NSC proliferation as well as fate and functional integration. However, the underlying mechanisms how NSCs react to extrinsic signals and convert them to intracellular responses still remains elusive. NSCs contain a functional endocannabinoid system, including the cannabinoid type-1 receptor (CB1). To decipher whether CB1 regulates adult neurogenesis directly or indirectly *in vivo*, we performed NSC-specific conditional inactivation of CB1 by using triple-transgenic mice. Here, we show that lack of CB1 in NSCs is sufficient to decrease proliferation of the stem cell pool, which consequently leads to a reduction in the number of newborn neurons. Furthermore, neuronal differentiation was compromised at the level of dendritic maturation pointing towards a postsynaptic role of CB1 *in vivo*. Deteriorated neurogenesis in NSC-specific CB1 knock-outs additionally resulted in reduced long-term potentiation in the hippocampal formation. The observed cellular and physiological alterations led to decreased short-term spatial memory and increased depression-like behavior. These results demonstrate that CB1 expressed in NSCs and their progeny controls neurogenesis in adult mice to regulate the NSC stem cell pool, dendritic morphology, activity-dependent plasticity, and behavior.

Key words: adult neurogenesis, CB1, mouse hippocampus, neural stem cells, neurogenesis-dependent behavior

Adult-born neurons are continuously generated in two zones of the mouse brain throughout life, in the subgranular zone (SGZ) of the dentate gyrus (DG) and in the subventricular zone (SVZ) of the lateral ventricle (Aimone et al. 2014; Bond et al. 2015). Newborn neurons in the SGZ migrate into the granule cell layer and are incorporated in the hippocampal circuitry to regulate multiple physiological functions (Dupret et al. 2007; Danielson et al. 2016; Anacker and Hen 2017; Toda et al. 2018), and furthermore, contribute to hippocampal plasticity (Toda and Gage 2018). Whether adult neurogenesis occurs in all mammals including humans is still under debate. Absence of adult neurogenesis was shown in cetaceans (Patzke et al. 2015). Additionally, three very recent publications were unable to demonstrate robust generation of newborn neurons in the adult human brain (Dennis et al. 2016; Cipriani et al. 2018; Sorrells et al. 2018), though another publication in 2018 came to the opposite conclusion and reported lifelong neurogenesis in humans (Boldrini et al. 2018), supporting evidences from earlier publications (reviewed in Kempermann et al. 2018).

The process of neurogenesis in the adult mouse brain is comprised of slowly dividing radial glial cells (type-1 cells) and the rapidly amplifying neural progenitor cells (NPCs, type-2 cells), which differentiate into neuroblasts and later into mature granule neurons with dendritic arborizations toward the molecular layer of the DG, and axonal projections toward the CA3 region (Toni and Schinder 2015; Pilz et al. 2018). Hippocampal adult neurogenesis is tightly controlled by the unique local microenvironment of the SGZ, where a multitude of signals converge to dynamically modulate the neural stem cell (NSC) niche. Although many extracellular signals, such as neurotrophins, neurotransmitters, cytokines, and hormones, are known to be involved in the regulation of NPC proliferation and differentiation (Mu et al. 2010; Goncalves et al. 2016), the precise extrinsic and intrinsic mechanisms involved in proliferation and cell fate determination remain to be fully elucidated. Many growth factors, such as epidermal growth factor (EGF) and basic fibroblast growth factor (bFGF), act as key regulators of NSC proliferation and differentiation (Temple 2001; Kempermann 2011). In addition, a variety of signals participate in the regulation of NPC differentiation to either neurogenesis or gliogenesis (Bond et al. 2015). In the past years, growing evidence has evolved that the endocannabinoids N-arachidonoylethanolamine (anandamide) and 2-arachidonoylglycerol (2-AG) as well as exogenous cannabinoids affect adult neurogenesis (Jiang et al. 2005; Marchalant et al. 2009; Wolf et al. 2010; Campos et al. 2013). Furthermore, modulation of endocannabinoid synthesis by either knocking out or inhibiting diacylglycerol lipase (DAGL) leads to a reduction of neurogenesis in both adult neurogenic zones (Gao et al. 2010; Oudin, Gajendra, et al. 2011). It has been demonstrated that adult NSCs contain a functional endocannabinoid system, which includes, besides the endocannabinoid synthesizing and degrading enzymes, the cannabinoid type-1 receptor (CB1) (Aguado et al. 2005; Galve-Roperh et al. 2007). CB1 is one of the most abundant G-protein coupled receptors in the brain with high expression levels in multiple neuronal subtypes (Marsicano and Kuner 2008). However, mature granule neurons in the dentate gyrus do not express CB1 (Monory et al. 2006), which could suggest that CB1 serves as an important regulator of adult NSCs and NPCs. Generally, CB1 has multiple functions, which are the inhibition of neurotransmitter release and the activation of different intracellular signaling cascades (Araque et al. 2017; Kendall and Yudowski 2017). Activation of CB1 leads to different cellular functions such as neuroprotection during epilepsy (Marsicano et al. 2003), cell lineage commitment (Bertrand et al. 2002), migration (Mulder et al. 2008), survival (Galve-Roperh et al. 2008; Díaz-Alonso et al. 2017), and neurite outgrowth (Berghuis et al. 2007) of developing neural cells. The observed effects of activated CB1 could be either explained via action on cells outside of the NSC lineage (indirect) through its modulatory role on neurotransmitter release, or direct via action on cells within the NSC lineage (i.e., NSCs, precursors, neuroblasts, neurons). Signaling through the PI3K/Akt and ERK pathways, downstream targets could involve the mammalian target of rapamycin complex 1 (mTORC1) and the cAMP response element-binding protein (CREB), which are central regulators of immediate early genes, such as c-fos, c-jun, zif268, and brain-derived neurotrophic factor (BDNF) (Pagotto et al. 2006; D'Souza et al. 2009; Gowran et al. 2011; Prenderville et al. 2015).

Intriguingly, CB1-deficient mice display reduced adult hippocampal neural precursor proliferation and decreased astroglial differentiation *in vitro* and *in vivo* (Jin et al. 2004; Aguado et al. 2006; Dubreucq et al. 2010). However, it is still unclear whether CB1 regulates adult NSCs through direct signaling in NSCs or an indirect mechanism via surrounding cells, e.g., by modulated neurotransmitter release from glutamatergic and/or GABAergic neurons, whereas both effects are not mutually exclusive. Indeed, neurotransmitters have been shown to affect the process of adult neurogenesis, and although the role of glutamate is less clearly delineated (Prenderville et al. 2015), the ability of GABA to reduce proliferative capacity is well established (Song et al. 2013).

To better understand the mechanism of CB1 in adult neurogenesis, we conditionally knocked-out CB1 (encoded by *CNR1*) in adult NSCs. So far, only a few studies were able to show a direct receptor gene function in regulating SGZ neurogenesis. One of the few examples is the conditional deletion of the FGF receptor *FGFR1* (Zhao et al. 2007) impairing NPC proliferation in the DG of adult mice. Furthermore, the study of Bergami and colleagues (Bergami et al. 2008) demonstrated that conditional NPC-specific deletion of *TrkB* led to compromised dendritic development and survival capacity of immature neurons, and BDNF-TrkB signaling has been shown to be imperative for hippocampal NSC proliferation in mice (Li et al. 2008). By using an inducible nestin-Cre mouse line we assessed the impact of NSC lineage-specific CB1 deletion on proliferation and differentiation of adult hippocampal NSCs, long-term potentiation, and hippocampus-dependent behavior. Our present study shows that proliferation of adult NSCs critically depends on activation of CB1 within the NSC lineage itself *in vivo* and reveals its remarkable impact on functional connectivity and involvement in behavior.

Material and methods

Animals

CB1-floxed (Marsicano et al. 2003), ROSA-stop-YFP (Srinivas et al. 2001) and nestin-CreERT2 (Corsini et al. 2009) mice were bred, in order to finally generate nes-CB1ko/ko mice (containing homozygous CB1-floxed/floxed alleles, homozygous ROSA-stop-YFP alleles, heterozygous nestin-CreERT2 allele) and control CB1wt/wt mice (containing homozygous CB1-wt/wt alleles, homozygous ROSA-stop-YFP alleles, heterozygous nestin-CreERT2 allele) (in C57BL/6 N background). Eight week old male mice were used for the study. Animals were single housed in a temperature- and humidity-controlled room with a 12 h light dark cycle (lights on 5 am - 5 pm) and had access to food and water *ad libitum*. All experiments were carried out in accordance with the European Community's Council Directive of 22

September 2010 (2010/63EU) and were approved by the local animal care committee (Landesuntersuchungsamt Koblenz, permit number G 13-1-093 and G 16-1-018). Experimenters were blind to the genotype of mice.

Tamoxifen and BrdU administration

Eight weeks old nes-CB1ko/ko and CB1wt/wt mice were administered tamoxifen (TAM) at 60 mg/kg/d for 5 days (intraperitoneal (i.p.); dissolved in 10% EtOH/90% sunflower oil). To examine the survival, proliferation, and differentiation of targeted cells, mice were injected for 5 days with bromodeoxyuridine (BrdU, 50 mg/kg/d) 23 days after TAM treatment. Mice were killed either one or 28 days after BrdU injections.

Production of recombinant lentivirus

High titer lentiviral particles were produced in 293LTV cells by transient transfection with calcium phosphate of transfer vector HS1-Cre (Suh *et al.*, 2007), second-generation packaging construct pCMV-deltaR8.91, and vesicular stomatitis virus envelope-expressing construct pMD2.G. 72 h after transfection, the supernatant was collected and purified by ultracentrifugation. The pellet was resuspended in PBS and aliquots stored at –80°C until use. The amount of transducing units was determined by diluting serially concentrated lentivirus into cell medium, plating and growing for 3 days. Cells were immunocytochemically stained and clones per sample were counted. Measurement of p24 concentration was carried out with the HIV-1 p24 ELISA assay (BioCat, Heidelberg, Germany).

Lentivirus vector administration

Adult mice were anesthetized by an i.p. injection of a combination of fentanyl (0.05 mg/kg), midazolam (5 mg/kg), and medetomidin (0.5 mg/kg). Mice were positioned in a stereotactic apparatus and kept on an animal heating pad to control body temperature during surgery. The scalp was cut open in rostrocaudal direction and lidocaine spray was applied on the skull and the surrounding skin to reduce pain. 1 µL of the lentivirus (1.4 × 1013 tu/mL) was injected bilaterally into the dentate gyrus at the following coordinates from bregma: –2.0 mm anteriorposterior, ±2.0 mm mediolateral, –2.0 dorsoventral. The virus was applied using a microprocessor controlled minipump with a 34G beveled NanoFil needle at a flow rate of 200 nL/min. The injection needle was left in place for additional 5 min and then slowly removed. After sewing the scalp, anesthesia was antagonized by intraperitoneal injection of flumazenil (0.5 mg/kg), naloxon (1.2 mg/kg) and atipamezol (2.5 mg/kg). Additionally, mice received a subcutaneous injection of buprenorphine (0.05 mg/kg) to reduce pain and 1 ml of 0.9% saline to compensate fluid loss during and after surgery. The mice were returned to their home cages, which were kept on a heating plate at 37°C overnight.

Immunohistochemistry

For immunohistochemistry, mice were perfused transcardially with 4% paraformaldehyde (PFA), brains were removed, postfixed overnight in 4% PFA and treated with 30% sucrose for 48 h. Then, brains were sectioned 30 µm thick in coronal plane and stored at 4 °C in cryoprotection solution until use.

Sections were blocked in phosphate buffered saline (PBS) containing 5% normal donkey serum (NDS), 2.5% bovine serum albumin (BSA) and 0.3% Triton X-100 (TX) for 90 min and incubated with the respective primary antibody in PBS containing 1% NDS, 0.1% BSA and 0.3% TX overnight. To double-stain with an anti-BrdU antibody, slides were fixed again for 15 min in 4% PFA to stabilize antigen-first primary antibody complexes. Sections were then incubated in 1 N HCl for 1 h at 37 °C to denature DNA, followed by 3 × 5 min washes with TBS. Brain slices were then blocked in tris buffered saline (TBS) with 1% NDS, 0.1% BSA and 0.3% TX for 90 min and incubated with primary antibodies in blocking buffer overnight at 4 °C. On the next day, appropriate secondary antibodies were applied for 2 h. To visualize cell nuclei in non-BrdU treated sections, brain slices were incubated with 4′,6-diamidino-2-phenylindole (DAPI) for 5 min, washed with PBS and mounted with Mowiol onto slides.

The following primary antibodies were used: rat anti-BrdU (1:100, Abcam), rabbit anti-GFP (1:500, kind gift of Matthias Klugman, Sydney, Australia), chicken anti-GFP (1:1000, Aves Labs), rabbit anti-RFP (1:500, Rockland), guinea pig anti-DCX (1:500, Merck), mouse anti-NeuN (1:500, Abcam), rabbit anti-S100b (1:500, Abcam), rabbit anti-CB1 (1:1000, Immunogenes), rabbit anti-CALB (1:5000, Swant), rabbit anti-cleaved Casp3 (1:200, Cell Signaling), mouse anti-GAD67 (1:500, Millipore). Mouse anti-CALR antibody (1:1000, Millipore) was used after antigen retrieval at 98 °C for 15 min in sodium citrate buffer (10 mM sodium citrate, 0.05% Tween 20, pH 6.0).

The respective secondary antibodies were applied: anti-rabbit IgG AlexaFluor488, goat anti-rabbit, goat anti-guinea pig, goat anti-rat AlexaFluor546 and goat anti-rabbit or anti-rat AlexaFluor647 (all 1:1000, Invitrogen).

Microscopic analysis of histology

Morphological and immunohistochemical analysis were performed with brains of naïve animals, which did not undergo behavioral tests before.

Cells were quantified in the hippocampus of each animal based on the Cavalieri principle of stereology. Every sixth atlas-matched, coronal hippocampal section located between 1.2 and 2.3 mm posterior to bregma, which comprises the dorsal and mid-dorsoventral part of the hippocampus, was used. The number of cells was normalized to the area of the dentate gyrus of each 30 µm section, followed by the determination of the total positive cell number in the 1080 µm analyzed region per animal. This was achieved by multiplying the counted cell number in each analyzed 30 µm section with 6 and then summarizing the total cell number per 180 µm region. Accordingly, the SVZ was analyzed (Supplementary data) comprising the region between 1.18 anterior to 0.02 mm posterior to the bregma.

Slides were observed under a Leica DM5500 fluorescence microscope or a Zeiss Axiovert LSM 710 laser scanning confocal microscope. For laser scanning confocal microscopy, z-stacks with optical sections of 1 µm were recorded.

YFP-positive cell numbers and co-localization with specific markers were counted in every sixth section (180 µm apart) and calculated based on the Cavalieri principle of stereology for the DG. For each marker four to six animals were analyzed.

Dendritic morphology and axonal growth

For dendritic analysis, animals were injected with TAM for 5 days. On the next day 1 µl of retrovirus CAG-DsRedExpress2 (Deshpande et al. 2013) with a titer in the range of 6.6×10^{10} to 2×10^{12} tu/ml (kindly provided by M. Götz, Munich) was injected

bilaterally into the dentate gyrus. Animals were perfused 28 days post infection (dpi), and brains were cut in 100 µm thick sections. Sections were immunostained with anti-RFP, anti-GFP, and anti-NeuN antibodies.

Z-series at 1.5 µm intervals were acquired by confocal microscopy with a 40x oil objective. The signal from immunoreactive intact neuronal dendrites was traced with Fiji by the NeuronJ plugin. The length of dendritic arbors was analyzed, and Sholl analysis was performed with the Sholl analysis plugin for Fiji. Dendritic spines were revealed by a 100x oil objective and z-stacks were acquired at 0.5 µm intervals in a total of 3–6 µm thickness. The number of spines was counted manually on the 2D maximum intensity projections, and spine density was calculated by dividing the number of dendritic protrusions by the total length of the analyzed segment (10–47 µm length).

For analysis of axonal growth, sections were photographed with the Perkin Elmer Opera Phenix HCS system in 1 µm z-intervals (total thickness 100 µm) with a 20x water objective. Maximum intensity projections were used to score axonal length by tracing fibers from the dentate to the end of axons in the CA3 region as previously reported (Zhao et al. 2006; Bergami et al. 2008). Measurement was performed by Fiji.

Electrophysiology

In vitro extracellular recordings were performed on acute hippocampal slices of wild-type control (CB1wt/wt) and CB1 KO animals (nes-CB1ko/ko). Mice were injected with Tamoxifen for five consecutive days at an age of eight weeks. Electrophysiological recordings were performed 4–6 weeks later. In-between animals were housed in a temperature- and humidity-controlled room with a 12 h light-dark cycle and had access to food and water ad libitum.

Electrophysiology: medial perforant path – DG

Transverse hippocampal slices (300 µm) were prepared from the dorsal hippocampus of 12–14 week old mice. Slices were incubated in oxygenated sucrose-containing artificial cerebrospinal fluid (ACSF) for 2 to 3 h and then transferred into oxygenated ACSF used for recordings. Composition of sucrose-containing ACSF: 85 mM NaCl, 75 mM sucrose, 2.5 mM KCl, 25 mM glucose, 1.25 NaH_2PO_4, four $MgCl_2$, 0.5 $CaCl_2$, and 24 $NaHCO_3$; composition of recording ACSF: 126 mM NaCl, 2.5 mM KCl, 26 mM $NaHCO_3$, 2 mM $CaCl_2$, 2 mM $MgCl_2$, 1.25 mM NaH_2PO_4, and 10 mM glucose. As specified in the results, in a subset of experiments, ifenprodil (3 µM; Tocris Bioscience) or picrotoxin (50 µM, Sigma-Aldrich) were added to the recording ACSF 20 min before to start the recordings and maintained throughout the recording time.

To elicit field excitatory postsynaptic potentials (fEPSPs) in the DG, a concentric bipolar stimulating electrode was placed in in the medial molecular layer of the upper blade of the DG to stimulate the afferent fibers of the medial perforant path (MPP). Input/output curves were obtained and the stimulation intensity producing ~50% of maximal response was used for test pulses and LTP induction. Baseline fEPSP were recorded for 20 min with a frequency of one test stimulus every 30 s. LTP was induced by tetanic stimulation that consisted of four trains of 100 Hz lasting 500 ms each, repeated every 20 s. After LTP induction, fEPSP were recorded every 30 s for additional 60 min. Slices were visualized with an upright microscope (Olympus; BX61WI) with infrared–differential interference contrast (IR-DIC) optics. All electrophysiological recordings were done at 33 °C. MultiClamp700B amplifier (Molecular Devices) was used for recordings. Signals were filtered at 3 kHz using a Bessel filter and digitized at 10 kHz with a Digidata 1440 A analog–digital interface (Molecular Devices). The recorded traces were analyzed using Clampfit 10.2 (Molecular Devices).

Electrophysiology: Schaffer collaterals – CA1

Acute hippocampal transversal slices were prepared from individuals at an age of 12 weeks, four weeks after TAM treatment. Mice were anesthetized with isoflurane and decapitated. The brain was removed and quickly transferred into ice-cold carbogenated (95% O2, 5% CO2) ACSF containing 125.0 mM NaCl, 2.0 mM KCl, 1.25 mM NaH_2PO_4, 2.0 mM $MgCl_2$, 26.0 mM $NaHCO_3$, 2.0 mM $CaCl_2$, 25.0 mM glucose. The hippocampus was sectioned into 400 µm thick transversal slices with a vibrating microtome (Leica, VT1200S). Slices were maintained in carbogenated ACSF at room temperature for at least 1.5 h before being transferred into a submerged recording chamber.

Slices were placed in a submerged recording chamber and perfused with carbogenated ACSF (32 °C; (125.0 mM NaCl, 2.0 mM KCl, 1.25 mM NaH_2PO_4, 1.0 mM $MgCl_2$, 26.0 mM $NaHCO_3$, 2.0 mM $CaCl_2$, 25.0 mM glucose)) at a rate of 1.2 to 1.5 ml/min. fEPSPs were recorded in stratum radiatum of the CA1 region with a borosilicate glass micropipette (resistance 2–5 Ω) filled with 3 M NaCl at a depth of 150–200 µm. Monopolar tungsten electrodes were used for stimulating the Schaffer collaterals at a frequency of 0.1 Hz. Stimulation intensity was adjusted to 40% of maximum fEPSP slope for 20 min baseline recording. LTP was induced by applying theta-burst stimulation (TBS: 10 trains of four pulses at 100 Hz in a 200 ms interval, repeated 3 times).

Basal synaptic transmission properties were analyzed via input-output measurements and short-term plasticity was examined via paired pulse facilitation. The IO- measurements were performed either by application of a defined current values (25–- 250 µA) or by adjusting the stimulus intensity to certain fiber volley amplitudes (0.1–0.7 mV). PPF was performed by applying a pair of two closely spaced stimuli in different interstimulus-intervals (ISI) ranging from 10 to 160 ms.

Behavioral assays

Bodyweight was measured once per week to observe any effect of TAM treatment on the overall health of animals. Animals were separated and single-housed one week before the start of behavioral assays. All behavioral tests were performed during the light phase of the cycle, starting at 8 am.

Open field test

Mice were placed in the center of a white box (40 × 40 × 40 cm^3) at 90 lux and their behavior was video recorded for 15 min and tracked using EthoVision XT. The distance moved was analyzed.

Light/dark box test

The experimental setup comprises an open, white, brightly-illuminated (100 lux at entry site) compartment (40 × 27 × 40 cm^3) and a closed, black, dark compartment (40 × 13 × 40 cm^3). Mice were placed in the dark compartment and allowed to explore the arena freely for 5 min. The entries and the time spent in the lit compartment were used as parameters to assess aversive behavior (Chambers et al. 2004).

Spatial object recognition test

The test was performed in a Y-maze (three arms (30 × 10 cm) at 120° from each other made of gray PVC) at 10 lux in the center of the maze. The mazes were surrounded by spatial extra-maze cues (white paper with black shapes) and taped intra-maze cues. Mice were placed in the center of the Y-maze. Animals were habituated to the empty Y-mazes for 10 min on two consecutive days before testing. Testing consisted of acquisition, an inter-trial interval and a retrieval trial. During the acquisition trial, mice were allowed to explore two identical copies of an object for 10 min. The objects were glass salt shakers (10 cm height) and were placed 5 cm apart from the walls at the end of two arms. The retrieval trial started after the 30 min inter-trial interval. During the 10 min retrieval trial, one object was placed in the empty arm of the maze (relocated object). The position of the relocated object was counterbalanced among animals. The acquisition and retrieval trials were video recorded and the total distance measured with EthoVision. For each mouse, the time spent exploring either object was manually scored during the retrieval trial and the index of recognition was calculated:

Index of recognition (%) = (new position time/ total exploration time) *100

Mice that remembered the original spatial location of the objects were expected to explore more the relocated object, having an index of recognition higher than 50%.

Forced swim test

The forced swim test has been shown to be a measure of behavioral despair. Mice were placed in a beaker filled with water (23 °C) and were video recorded for 5 min. The behavior was analyzed manually. The immobility time was defined as the duration a mouse floating in the water without struggling and making only small movements to keep its head above the water.

Morris water maze

The Morris water maze is a spatial learning task originally developed for rats. A large circular tank (diameter 1.20 m) was filled with water (25 ± 1 °C) and the escape platform (diameter 10 cm) was submerged 1 cm below the surface. The animals were tracked with the Video Tracking System EthoVision XT.

During the first 2 days, mice were trained to swim to a visible platform (visible platform task) that was marked with a 15 cm high black flag and placed pseudo-randomly in different locations across trials (non-spatial training). The extra-maze cues were hidden during these trials. After 2 days of visible platform training, hidden platform training (spatial training) was performed.

The next following 8 days, mice had to navigate using extra-maze cues which were placed on the walls of the testing room. Mice were trained to find a hidden platform which was located at the center of the southwest quadrant of the pool. The location of the platform was the same throughout testing. Every day, mice performed four trials with an intertrial interval of 5 min. The animals were released into the water facing the pool wall randomly at one of four start locations and were allowed to swim until they find the platform, or for a maximum of 90 s. Any mouse that failed to find the platform within 90 s was guided to the platform. The animal then remained on the platform for 20 s before being removed from the pool. The day after completion of the hidden platform training, a probe trial was conducted in order to determine whether the mice had developed a spatial preference for the former platform quadrant. The platform was removed from the pool and the mice were allowed to swim freely for 90 s.

Statistical analysis

Data are represented as the mean ± standard error of the mean (SEM). Statistical analysis was done using GraphPad Prism 4 (GraphPad Software Inc, La Jolla, CA, USA) and IBM SPSS Statistics 22 v software (IBM Corporation, Armonk, NY, USA). Unless otherwise specified, data were analyzed using two-tailed unpaired Student's t-test. For Sholl analysis, repeated measures ANOVA followed by post hoc Bonferroni test for group comparison was used. The p-value used to determine significance was $P < 0.05$.

Results

Conditional deletion of CB1 from adult NSCs

To assess the direct influence of CB1 on regulating adult neurogenesis *in vivo*, we generated a triple-transgenic mouse line (Fig. 1A) by crossbreeding mice expressing a tamoxifen (TAM)-inducible Cre-recombinase under the NSC-specific nestin promoter and enhancer with floxed CB1 mice. To visualize recombined cells, the offspring was additionally crossed with the reporter mouse line ROSA26-floxed-stop-YFP. TAM treatment led to Cre-mediated excision of the floxed-stop cassette inducing YFP expression, and to Cre-mediated deletion of CB1, obtaining nes-CB1ko/ko. Control mice are called CB1wt/wt, containing Cre-mediated YFP expression after TAM treatment, but wild-type CB1 alleles. Recombination efficiency in CB1 and ROSA genomic loci was similar, as evaluated by genomic PCR analyzes in clonally-derived single DG-derived neurospheres from TAM treated mice (Supplementary Fig. 1). In further experiments, mice were injected with TAM at eight weeks of age and used for analyzes 28 or 56 days later (Fig. 1B). Recombination and expression of YFP occurred specifically in both neurogenic regions, in the SVZ (Fig. 1C) and the SGZ of the DG (Fig. 1D). In order to exclude unwanted ectopic recombination in GABAergic interneurons, we verified that the pool of forebrain CB1-expressing interneurons was unchanged in nes-CB1ko/ko as compared to CB1wt/wt control mice (Supplementary Fig. 2).

Quantification of YFP reporter-positive cells in the SGZ (Fig. 1E) showed that at 28 days post TAM treatment (dptm) in CB1wt/wt mice 11 700 ± 534 cells were YFP-positive. Significantly less ($P = 0.007$) YFP-positive cells were found in the SGZ of nes-CB1ko/ko mice (7823 ± 903). At 56 dptm, the number of YFP-positive cells was still reduced ($P = 0.048$) in nes-CB1ko/ko mice (10 600 ± 1375) compared to CB1wt/wt mice (14 660 ± 887). When performing a two-way analysis of variance (ANOVA) for time and genotype, we found a significant increase of YFP-positive cells by 56 dptm compared to 28 dptm ($P = 0.009$), and a significant genotype difference ($P = 0.001$). No interaction between time and genotype was observed, indicating that independent of the genotype an increase of labeled cells was found at the later time point.

To confirm that CB1 was deleted from YFP-positive cells, we immunostained sections from CB1wt/wt and nes-CB1ko/ko with YFP and CB1 specific antibodies (Fig. 1F). CB1 was not detected anymore in recombined YFP-positive cells of nes-CB1ko/ko mice.

Deletion of CB1 reduces proliferation capacity of newborn cells

Since nes-CB1ko/ko animals displayed a decreased number of YFP-positive cells, we investigated the maturation stage of the cells by quantifying YFP-positive cells co-expressing cell type-specific antigens at 28 dptm and 56 dptm. At 23 dptm, we

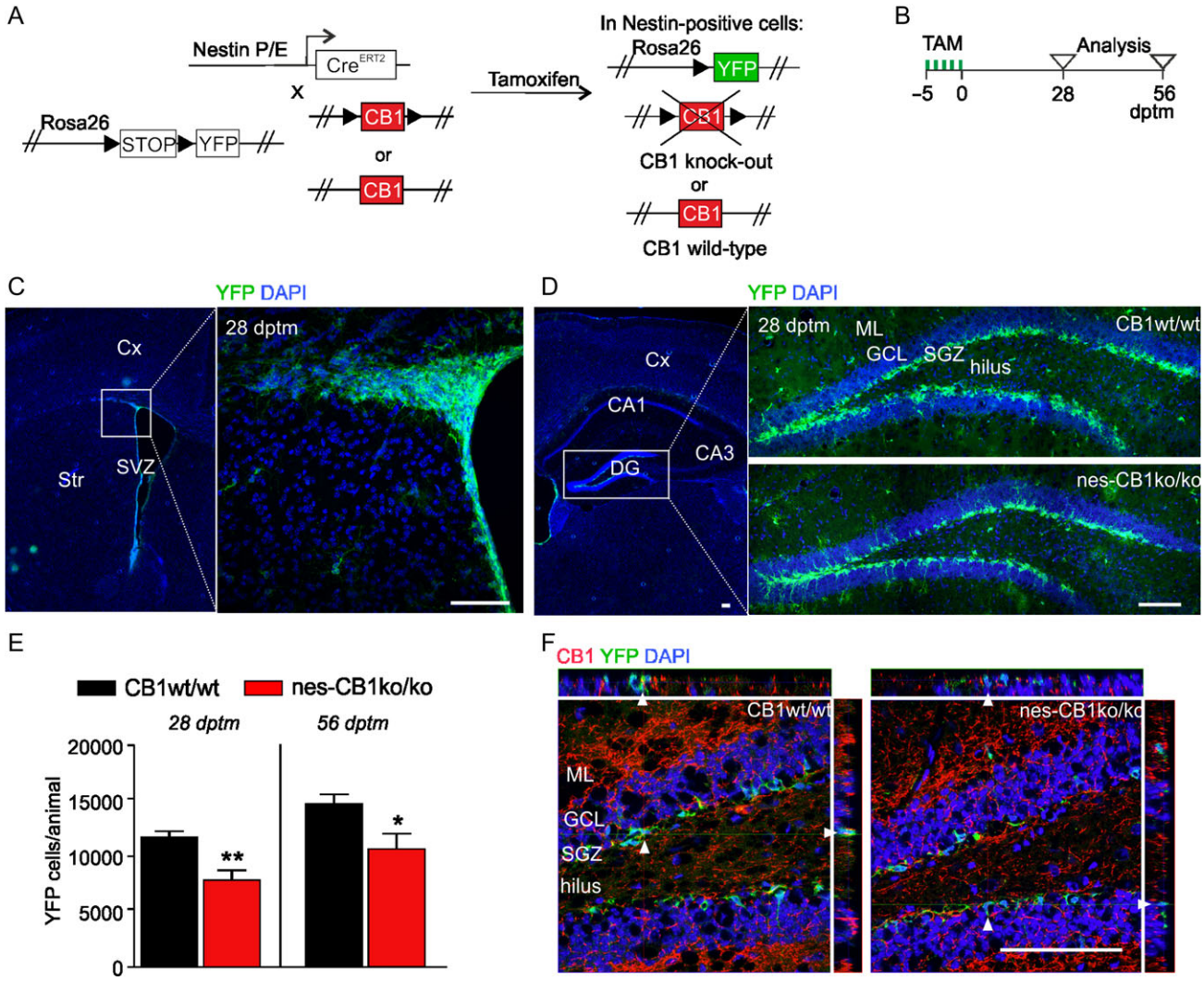

Figure 1. (A) Scheme of the strategy for conditional deletion of CB1 from NSCs and genetic tagging of NSC with YFP *in vivo* (using nes-CreERT2, expressing tamoxifen-inducible Cre under the control of nestin promoter/enhancer elements, P/E), obtaining nes-CB1ko/ko. The respective controls (CB1wt/wt) contain the wild-type CB1 alleles, but are YFP tagged. (B) Time course of experiment. Mice were perfused at 28 days post tamoxifen-induced recombination (dptm) or 56 dptm. (C) Recombined cells express YFP (green) and are present in the subventricular zone (SVZ) and (D) in the subgranular zone (SGZ) of the dentate gyrus (DG). (E) Quantification of YFP-positive cells in the DG revealed a significant decrease in nes-CB1ko/ko mice as compared with CB1wt/wt at 28 dptm and 56 dptm. $n = 4$ animals/group, $^{**}P < 0.01$, $^{*}P < 0.05$, two-tailed unpaired Student's t-test. Data are represented as mean ± SEM. (F) Representative confocal images including z-stacks display co-localization of recombined YFP cells (green) and CB1 expression (red) in CB1wt/wt mice, whereas nes-CB1ko/ko mice show a lack of CB1 expression in recombined YFP cells (arrowheads indicate corresponding points in the orthogonal planes). DAPI, blue. Scale bar, 100 μm. Cortex (Cx); Striatum (Str); granule cell layer (GCL), molecular layer (ML).

injected BrdU for five consecutive days to follow the proliferation and fate of recombined cells (Fig. 2A).

At 28 dptm, we found recombined YFP cells either positive for doublecortin (DCX), NeuN or S100b as assessed by immunostaining in both genotypes (Fig. 2B). Furthermore, a population of YFP-positive cells was marked by anti-BrdU immunoreactivity (Fig. 2C). Four weeks later (56 dptm), YFP cells still co-expressed the aforementioned markers (Fig. 2D). When we quantified the co-localizing cells, we found at 28 dptm 6424 ± 427 cells in CB1 wt/wt mice expressing the marker of developing neurons DCX, whereas 4388 ± 620 cells in nes-CB1ko/ko were positive for DCX, representing a decreased ($P = 0.035$) pool of neuroblasts. At this stage, 2178 ± 450 cells in CB1wt/wt mice were positive for the marker NeuN, but only 716 ± 250 cells in nes-CB1ko/ko mice, demonstrating additionally a significantly decreased ($P = 0.047$) number of mature neurons (Fig. 2E). Also, YFP cells positive for S100b, marking the astroglial lineage, were significantly reduced at 28 dptm in nes-CB1ko/ko mice ($P = 0.021$), with 1800 ± 292 cells as compared to 2890 ± 24 cells in CB1wt/wt animals. At 56 dptm, the YFP/S100b-positive astrocytic population was much smaller (546 ± 81 cells in CB1wt/wt, 408 ± 79 cells nes-CB1ko/ko mice), without significant genotype differences ($P = 0.269$), but same trend as at 28 dptm.

In contrast to the astrocytic YFP cells, the pool of both neuronal populations (DCX+ and NeuN+) increased in wild-type and mutant animals at 56 dptm. 6992 ± 681 YFP-positive cells were positive for DCX in the CB1wt/wt animals, while only 4358 ± 587 cells were positive for DCX in nes-CB1ko/ko mice ($P = 0.026$). Furthermore, nes-CB1ko/ko animals showed a decreased ($P = 0.029$) number of YFP/NeuN double positive cells (3773 ± 84) compared to CB1wt/wt mice (6828 ± 851) (Fig. 2E). Furthermore, we addressed the stage-specific markers calretinin (CALR), which generally starts to get expressed 14 days after neuron birth in the SGZ, and calbindin (CALB), starting to be expressed

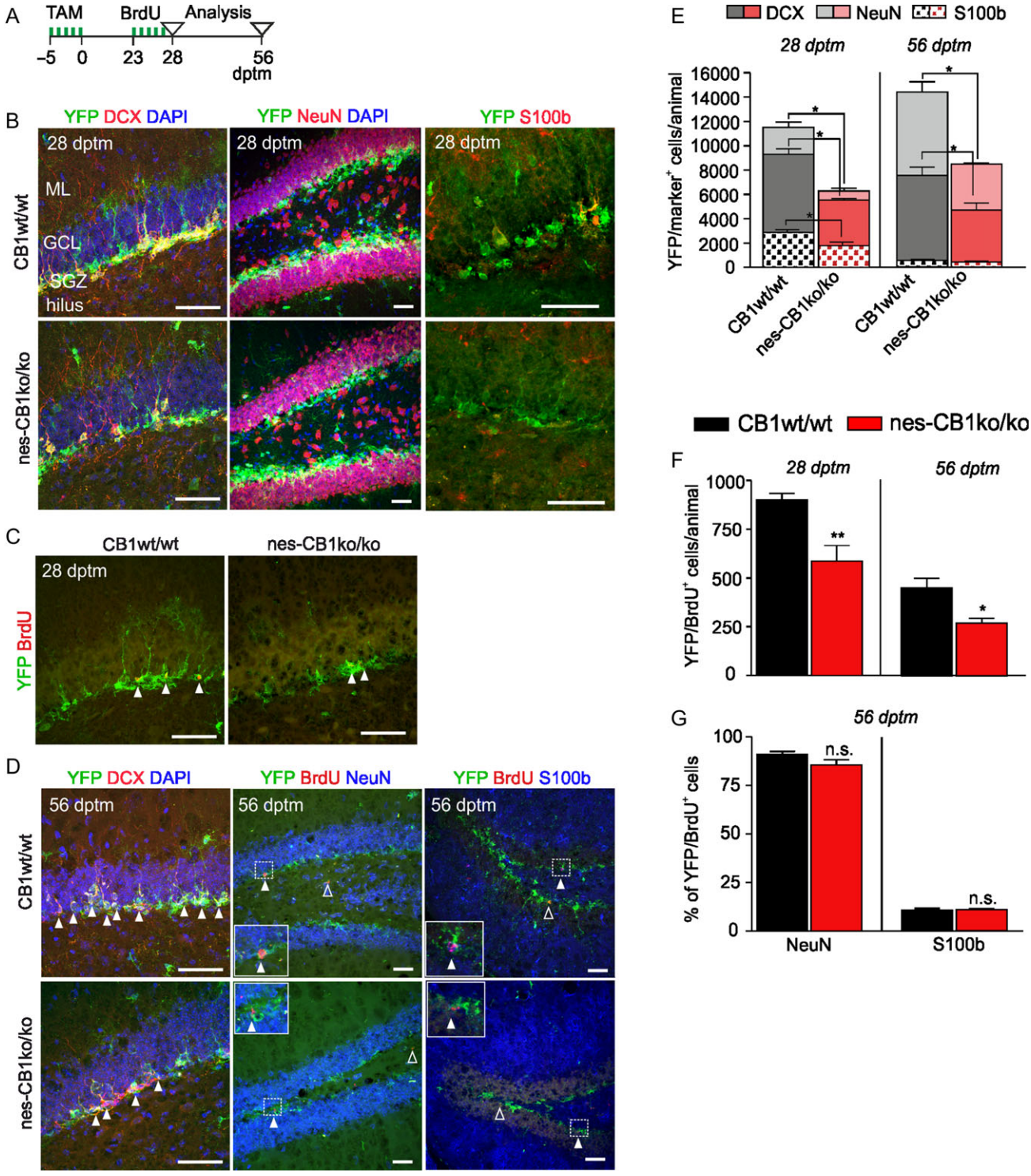

Figure 2. (A) Schedule of experiment. Mice were injected with BrdU for five d at 23 dptm and were analyzed at 28 dptm and at 56 dptm, respectively. (B) Maximum intensity projections of z-stacks show YFP-positive cells expressing DCX, NeuN or S100b at 28 dptm. (C) Maximum intensity projections of z-stacks show YFP expressing cells positive for BrdU at 28 dptm (filled arrowhead: colocalizing cell). (D) Triple co-localization (filled arrowhead) at 56 dptm (with magnification in the quadrant), empty arrowhead: positive YFP/BrdU cell. (E) Quantification of YFP-positive cells co-localizating with the neuronal and astrocytic markers. Deletion of CB1 reduces the YFP/DCX and YFP/NeuN population at 28 dptm and 56 dptm. YFP/S100b cells were significantly reduced only at 28 dptm. $n = 5$ (28 dptm S100b), $n = 3$ (28 dptm DCX), $n = 4$ (28 dptm NeuN), $n = 4$ (56 dptm S100b), $n = 4$ (56 dptm DCX), $n = 4$ (56 dptm NeuN) animals/group $^{*}P < 0.05$, $^{**}P < 0.01$, two-tailed unpaired Student's t-test. (F) Nes-CB1ko/ko animals displayed a significantly reduced number of newborn cells, as assessed by co-localization of YFP with BrdU. $n = 5$ (28 dptm CB1wt/wt), $n = 6$ (28 dptm nes-CB1ko/ko), $n = 4$ (56 dptm CB1wt/wt), $n = 4$ (28 dptm nes-CB1ko/ko) animals/group; $^{*}P < 0.05$, $^{**}P < 0.01$, two-tailed unpaired Student's t-test. (G) Differentiation of BrdU labeled cells into the neuronal (NeuN) or astroglial (S100b) lineage is not affected at 56 dptm. $N = 4$ animals/group, two-tailed unpaired Student's t-test, n.s. not significant. Data represent mean ± SEM. Scale bar, 50 μm. Subgranular zone (SGZ), granule cell layer (GCL), molecular layer (ML).

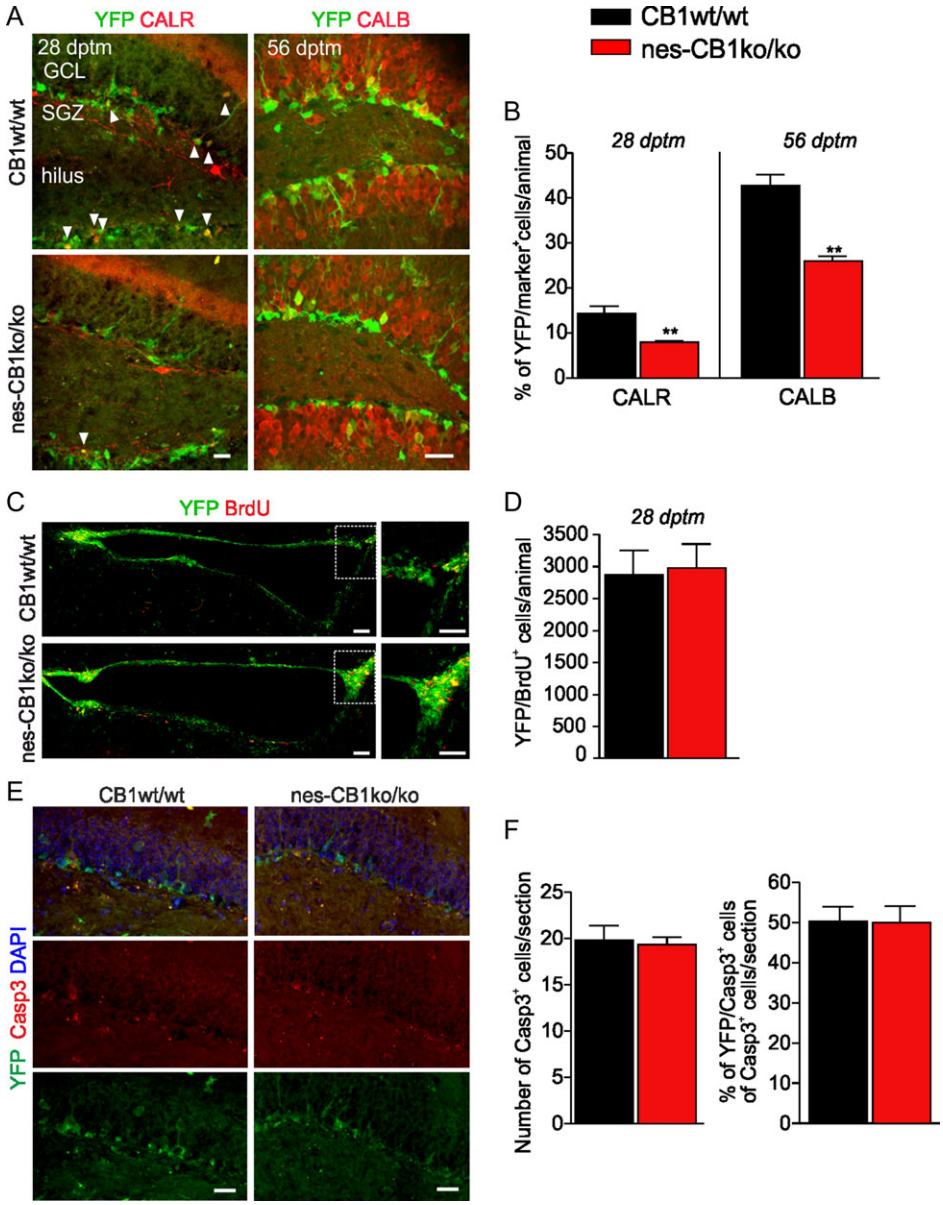

Figure 3. (A) Maximum intensity projections of z-stacks showing YFP- positive cells expressing calretinin (CALR) at 28 dptm (arrowhead: co-localizing cell) and calbindin (CALB) at 56 dptm. Scale bar, 20 µm. (B) Quantification of YFP cells co-localizing with the two stage-specific markers. Deletion of CB1 reduced the YFP/CALR-positive population at 28 dptm and YFP/CALB-positive population at 56 dptm. N = 4 animals/group *P < 0.05, **P < 0.01, two-tailed unpaired Student's t-test. (C) Maximum intensity projections of z-stacks showing YFP/BrdU-positive cells in the SVZ at 28 dptm, overview and magnified area of the rectangle in the overview. Scale bar, 50 µm. (D) Quantification of anti-BrdU and anti-YFP co-staining in the SVZ demonstrates no difference between CB1wt/wt and nes-CB1 ko/ko animals. (n = 4 for CB1wt/wt, n = 5 for nes-CB1ko/ko). (E) Exemplary micrographs showing apoptotic cells evaluated by activated caspase-3 (Casp3) staining and YFP-positive cells in CB1wt/wt and nes-CB1ko/ko mice at 28 dptm. Scale bar, 20 µm. (F) Averaged number of Casp3-positive cells in the DG per hippocampal section (left panel) and percentage of YFP/Casp3-positive cells of all Casp3-positive cells per section (right panel) at 28 dptm. N = 4 animals per genotype (CB1wt/wt: n = 13 sections; nes-CB1ko/ko: n = 19 sections).

approximately after one month (Zhao et al. 2008). When analyzing CALR at 28 dptm and CALB at 56 dptm, we also observed approximately half as many YFP co-expressing cells in nes-CB1ko/ko mice with these two maturation markers (Fig. 3A, B). At 28 dptm, 13.79 ± 1.54% of YFP-positive cells were positive for CALR in CB1wt/wt animals, whereas nes-CB1ko/ko animals displayed only 7.752 ± 0.35% double positive cells. At 56 dptm, 41.89 ± 2.61% cells were CALB/YFP-positive in CB1wt/wt and 25.71 ± 1.51% in nes-CB1ko/ko animals.

In order to generally analyze at which maturation state neuronal progenitors loose CB1 expression, as mature granule cells are devoid of it (Monory et al. 2006), we performed double FISH for CB1 and CALR, and CALB, respectively. ISH experiments revealed that CB1 is still expressed at the stage of CALR expression in developing newborn neurons (Supplementary Fig. 3) and is absent on further differentiated CALB-positive cells in the subgranular zone (Supplementary Fig. 4).

Since the deletion of CB1 from NSCs led to a decreased pool of astrocytes, neuroblasts, and neurons, we assessed the proliferation rate of the recombined cells (Fig. 2F). We found that in CB1wt/wt mice 900 ± 34 cells were YFP/BrdU-positive and only 586 ± 81 in nes-CB1ko/ko, representing a significant smaller

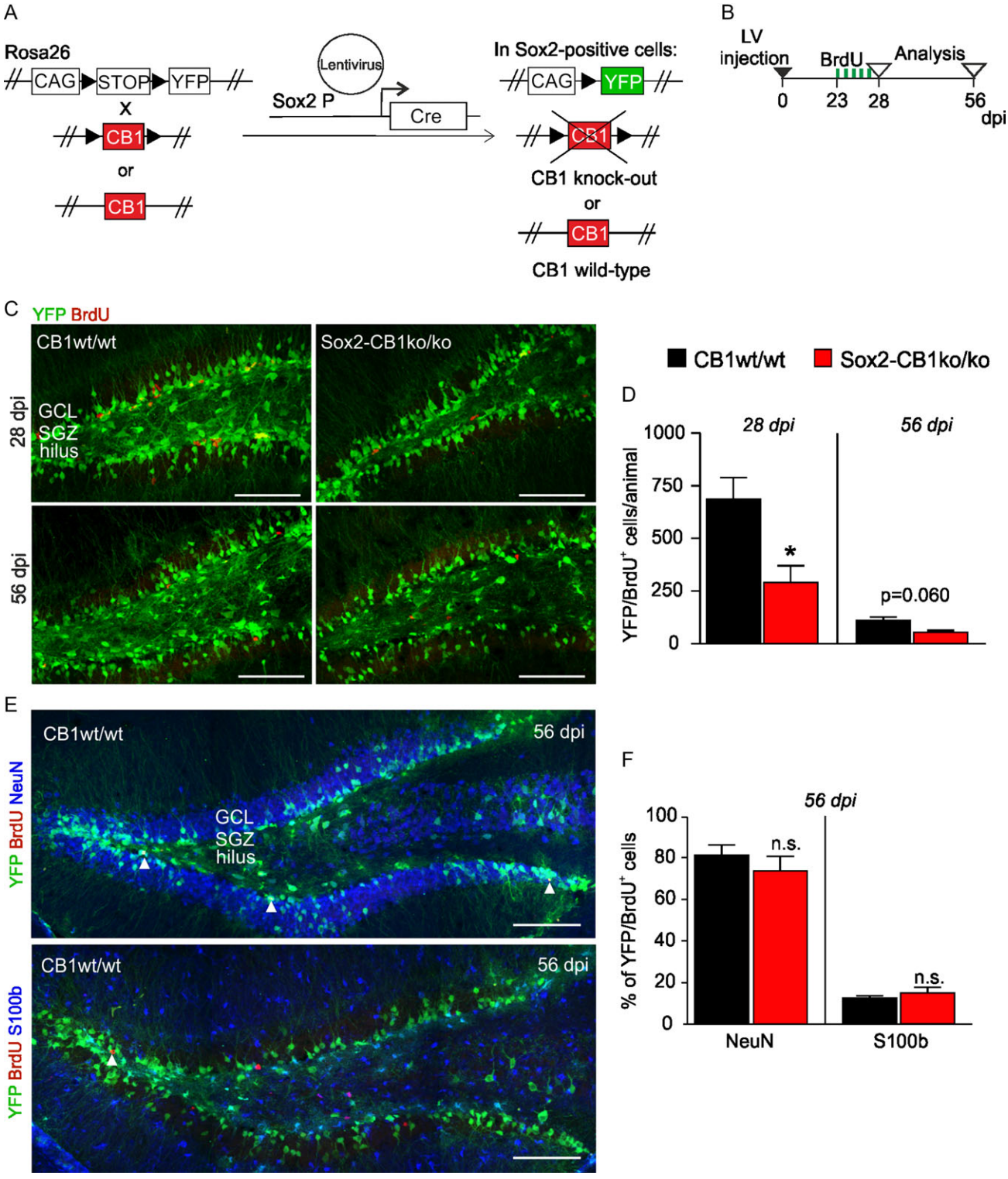

Figure 4. (A) Scheme of deletion of CB1 from neural stem cells *in vivo* with a lentivirus containing Cre recombinase under the control of the Sox2 promoter (Sox2 P), obtaining Sox2-CB1ko/ko. The respective controls (CB1wt/wt) contain the wild-type CB1 alleles, but are YFP tagged. (B) Experimental timeline. Eight weeks old animals were injected with the lentivirus (LV) via stereotactic surgery. BrdU was injected i.p. for five consecutive days starting at 23 dpi, and animals were perfused at 28 dpi and 56 dpi. (C) Representative micrographs of CB1wt/wt and Sox2-CB1ko/ko mice show recombined cells in the subgranular zone (SGZ) expressing YFP (green) after lentivirus injection and a fraction of it co-localizing with BrdU (red) at 28 dpi and at 56 dpi. (D) Quantification of YFP/BrdU double positive cells showed that CB1 loss impaired significantly cell proliferation (at 28 dpi), but maintenance of YFP/BrdU cells (at 56 dpi) is only slightly (but not significantly) decreased upon CB1 deletion ($P = 0.060$). $N = 3$ animals/group, $^*P < 0.05$, two-tailed unpaired Student's t-test, $t = 2.845$. (E) Exemplary micrographs of CB1wt/wt animals for YFP (green) cells co-localizing with BrdU (red) and S100b or NeuN (blue) in the dentate gyrus at 56 dpi. Arrowheads mark triple positive cells. (F) Percentage of YFP/BrdU/marker of total YFP/BrdU-positive cells (marker: S100b or NeuN) at 56 dpi. Differentiation into the astroglial or neuronal lineage is not affected. $N = 4$ (CB1wt/wt) and $n = 3$ (Sox2-CB1ko/ko) animals/group, n.s. not significant in two-tailed unpaired Student's t-test. Values represent mean ± SEM. Scale bar, 100 μm.

(P = 0.009) pool of proliferating cells at 28 dptm. In contrast, NSC-specific CB1-deletion did not alter proliferation of NSCs/NPCs in the SVZ (Fig. 3C, D). In order to test whether apoptosis could contribute to the reduction of BrdU-positive cells in the DG, we performed immunostaining against cleaved and therefore activated caspase-3. The data indicated that apoptosis was unchanged between both genotypes (Fig. 3E, F).

BrdU-positive cells in the DG were also counted four weeks after BrdU injection to measure their differentiation potential. At 56 dptm, 449 ± 51 cells expressed YFP/BrdU in CB1wt/wt mice, but only 269 ± 26 cells in nes-CB1ko/ko mice, demonstrating a significantly (P = 0.020) smaller amount of YFP/BrdU cells (Fig. 2F). Next, we determined the phenotype of YFP/BrdU cells by co-immunostaining with either the neuronal marker NeuN or the astroglial marker S100b (Fig. 2G). 91.0 ± 1.5% of YFP/BrdU cells in CB1wt/wt mice were positive for NeuN and 85.5 ± 2.7% in nes-CB1ko/ko mice. In contrast, 10.6 ± 0.9% of YFP/BrdU cells in CB1wt/wt mice were positive for S100b and 10.8 ± 0.6% in nes-CB1ko/ko mice. Thus, we found no difference between the two genotypes in the differentiation into the neuronal or astroglial lineage. Taken together, our results indicate that CB1 regulates the proliferation capacity, leading to a reduced number of neuroblasts and neurons, but also of astrocytes. CB1 itself does not alter directly the cell fate of adult NSCs.

These results are corroborated by using another genetic approach, in which we injected a lentivirus containing a Sox-2 promoter-driven Cre recombinase (Sox2-Cre) into the DG of ROSA26-floxed-stop-YFP mice crossed with floxed CB1 animals (Fig. 4A). Due to activity of Sox-2 promoter in NSCs, CB1 was knocked-out in NSCs, and YFP was expressed. At 23 days post infection (dpi), BrdU was injected to quantify the proliferation at 28 dpi and the differentiation at 56 dpi (Fig. 4B). Injection of Sox2-Cre lentivirus led to expression of YFP in adult NSCs and their progeny in the SGZ of the DG in both CB1wt/wt and Sox2-CB1ko/ko mice and to BrdU labeled dividing cells (Fig. 4C). YFP/BrdU-positive cells were reduced (P = 0.039) in Sox2-CB1ko/ko mice (289 ± 82 cells) 28 dpi as compared to CB1wt/wt mice (686 ± 103 cells). (Fig. 4D). At 56 dpi, YFP/BrdU cells were also decreased in Sox2-CB1ko/ko mice (53 ± 10 cells) as compared to CB1wt/wt mice (108 ± 18 cells), but not significantly (P = 0.06). Furthermore, we were interested in investigating the differentiation potential of targeted cells, using co-localization analysis of YFP-positive cells with either the astrocytic marker S100b or the neuronal marker NeuN (Fig. 4E). Quantification showed

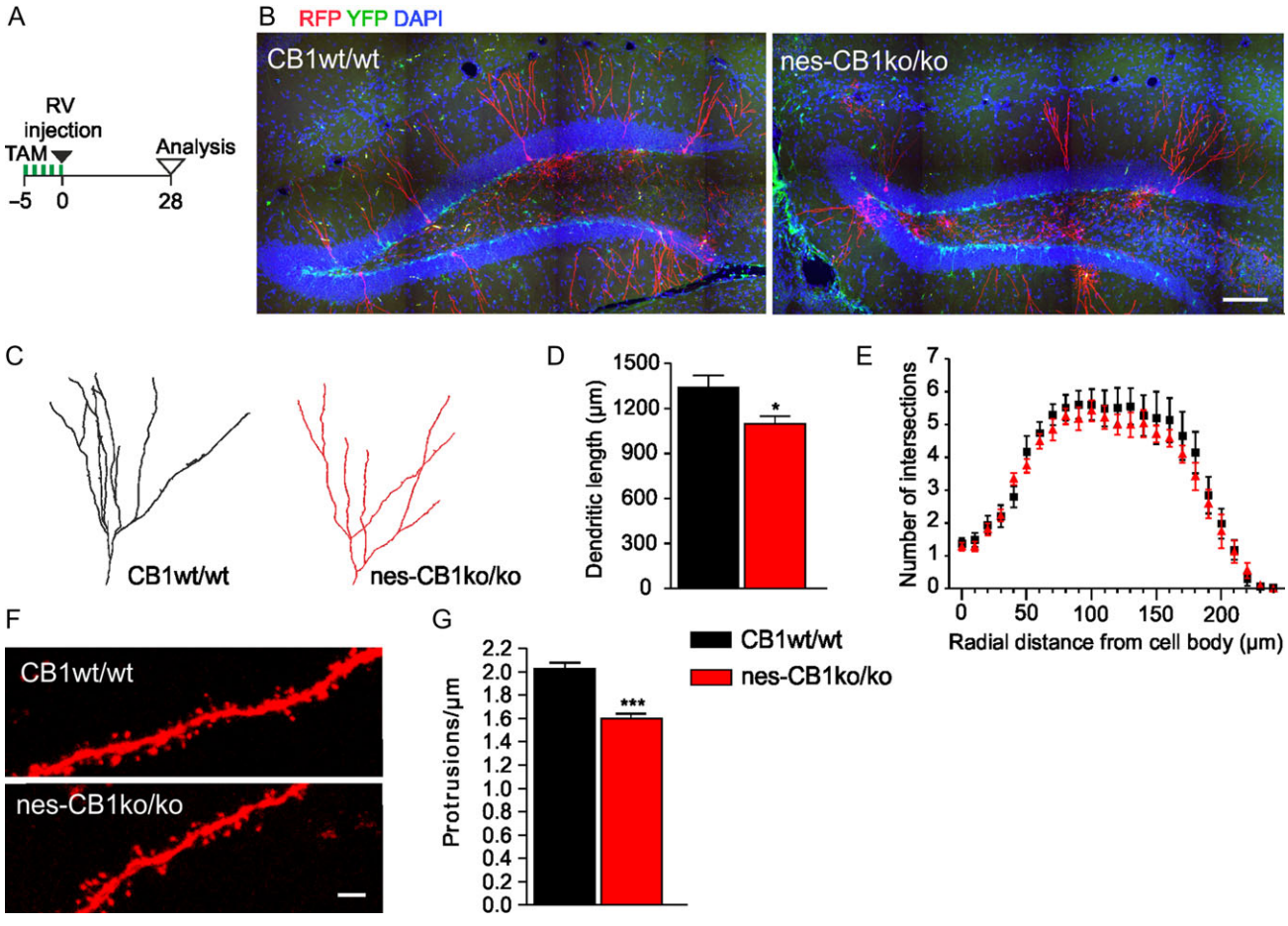

Figure 5. (A) Timeline showing the experimental paradigm used for retroviral injections into TAM-induced nes-CB1ko/ko and control mice. (B) Representative micrograph depicting recombined YFP cells and retrovirally-labeled RFP newborn neurons in the hippocampus in CB1wt/wt and nes-CB1ko/ko mice. (C) Maximum intensity projection of a three-dimensionally traced neuron in CB1wt/wt and nes-CB1ko/ko animals. (D) Histogram showing significantly reduced dendritic length of traced neurons in nes-CB1ko/ko mice as compared to CB1wt/wt control (n = 23 neurons; six animals per genotype); *P < 0.05, two-tailed unpaired Student's t-test. (E) Sholl analysis shows no alterations in number of intersections of dendritic arbors. Data represent mean ± SEM. Scale bar, 100 µm. (F) Exemplary micrographs showing dendritic filaments of retrovirally RFP-labeled newborn neurons in CB1wt/wt and nes-CB1ko/ko mice. Scale bar, 2 µm. (G) Graph depicting the quantification of protrusions in dendritic segments (n = 21 segments; four mice). The density of dendritic spines is expressed as protrusions per micrometer dendritic length; ***P < 0.0001, two-tailed unpaired Student's t-test.

81.0 ± 4.8% being triple positive for YFP/BrdU/NeuN in CB1wt/wt and 73.5 ± 7.1% in Sox2-CB1ko/ko mice, revealing no difference between both genotypes (Fig. 4F). In CB1wt/wt, 12.2 ± 1.3% were triple positive for YFP/BrdU/S100b and 14.7 ± 2.8% in Sox2-CB1ko/ko mice, indicating that differentiation into the astroglial lineage was not affected.

Dendritic, but not axonal growth is regulated by CB1 in newborn neurons

To examine if absence of CB1 has an effect on the integration of adult-born neurons into the existing neural circuitry, we analyzed the morphology of four-week old neurons. Mice were injected with a retrovirus transducing RFP on the last day of TAM treatment (Fig. 5A). On 28 dpi, single newborn neurons in the SGZ were visualized (Fig. 5B), with dendrites extending through the molecular layer of the DG. Three-dimensional reconstruction of the dendritic arbor in both CB1wt/wt and nes-CB1ko/ko mice (Fig. 5C) revealed a significantly reduced ($P = 0.03$) dendritic length in CB1-deficient neurons (1097 ± 52 µm) as compared to control neurons (1340 ± 81 µm) (Fig. 5D). To further analyze dendritic arborization, Sholl analysis was carried out in 4-week-old neurons, which revealed no significant differences in dendritic complexity between control and CB1-deficient neurons (Fig. 5E). However, dendritic spine density was significantly reduced in nes-CB1ko/ko (1.601 ± 0.064 protrusions/µm) as compared to CB1wt/wt (2.016 ± 0.05631 protrusions/µm) mice ($P < 0.0001$) (Fig. 5F and G). In contrast, measurement of axonal length revealed no difference between CB1wt/wt (1160 ± 34.43 µm, $n = 22$ sections of injected hemispheres, four mice) and nes-CB1ko/ko (1096 ± 46.3 µm, $n = 17$ sections of injected hemispheres, four mice) mice (Supplementary Fig. 5), pointing towards a CB1-independent mechanism of regulating axonal length in newborn hippocampal granule neurons.

Given that diacylglycerol lipase (DAGL), the major 2-AG synthesizing enzyme, and 2-AG signaling play a crucial role in dendritic elongation (Oudin, Hobbs, et al. 2011), we tested whether the observed defects in dendritic growth in nes-CB1ko/ko arise from a reduced DAGLα and 2-AG signaling. To this end, we FACS-isolated two distinct SGZ subpopulations, namely $CD133^+$ neural stem cells and PSA-$NCAM^+$ newborn neurons, in both genotypes and analyzed DAGLα expression by RT/qPCR. We did not detect a genotype difference in $CD133^+$ neural stem cells and, most importantly, neither in PSA-$NCAM^+$ newborn neurons (Supplementary Fig. 6). Interestingly, we found a genotype-independent, 3-fold upregulation of DAGLα in PSA-$NCAM^+$ cells as compared to $CD133^+$ neural stem cells.

To figure out more potential dysregulated candidate genes, which had been implicated in progenitor proliferation and neurite growth and could therefore account for the defects seen in nes-CB1ko/ko mice, we performed RT/qPCR experiments of DG neurospheres from both genotypes and found that BDNF mRNA levels were decreased in nes-CB1ko/ko (Supplementary Fig. 7). We furthermore addressed the question whether other components of the endocannabinoid system were dysregulated. In fact, CB2 mRNA levels were found to be reduced in nes-CB1ko/ko (Supplementary Fig. 7).

CB1 is required for neurogenesis-dependent LTP in the hippocampus

Adult neurogenesis involves incorporation of new neurons in the existing neural circuitry. Since we manipulated the proliferation potential of newborn neurons and the number of neuroblasts and neurons, a potential impact of CB1 deletion on circuit properties, including synaptic plasticity, was investigated. Specifically, we analyzed the development of long-term potentiation (LTP) induced by theta burst stimulation (TBS) at two hippocampal synapses: medial perforant path to dentate gyrus (MPP-DG) and CA3 to CA1 (CA3-CA1).

To study the potentiation of adult born granule cells, we first investigated LTP at the MPP-DG synapse in the presence of picrotoxin, a GABA-A receptor antagonist. In these conditions (i.e., in the presence of picrotoxin), LTP was indistinguishable between the two groups (Fig. 6A and C), suggesting that CB1 deletion does not change potentiation of adult granule neurons. New neurons in the DG have been shown to undergo a form of LTP, which requires the activation of NR2b subunit-containing NMDA receptors (Snyder et al. 2001). After TBS at MPP-DG synapses in the absence of picrotoxin, control mice displayed a potentiation lasting for 60 min, which was blocked when the NR2b antagonist ifenprodil was applied. In contrast, the level of potentiation in nes-CB1ko/ko mice was lower than in control mice, and the potentiation exhibited a decay similar to that observed in slices from control mice after incubation with ifenprodil (Fig. 6B). Averaged potentiation levels of the last 5 min displayed significantly different fEPSP slopes in nes-CB1ko/ko (103.5 ± 2.4%, $P = 0.007$) and CB1wt/wt+ifenprodil (99.4 ± 2.2%, $P = 0.008$) mice as compared to CB1wt/wt mice (120.1 ± 3.1%) (Fig. 6D).

To further analyze physiological changes in synaptic plasticity in the hippocampus of nes-CB1ko/ko mice, we stimulated Schaffer collaterals of CA3 by TBS and recorded fEPSPs in CA1, which resulted in an LTP that was significantly different from that of wild-type controls (Fig. 6E). Averaged potentiation levels of the last 5 min of LTP recording displayed significant different ($P = 0.042$) fEPSP slopes in nes-CB1ko/ko (132.47 ± 2.04%) mice as compared to CB1wt/wt mice (141.01 ± 2.98%) (Fig. 6F).

Baseline synaptic transmission in these LTP experiments was evaluated by testing input-output responses, and short-term plasticity was also tested by paired-pulse-paradigm (Supplementary Fig. 8). Basal synaptic properties in the DG were unaltered between the three groups (wt/wt; CB1ko/ko; wt/wt+ifenprodil) when slices were treated with picrotoxin (Supplementary Fig. 8A). Untreated slices from nes-CB1ko/ko animals showed significant alterations at fiber volley amplitudes between 0.3 and 0.5 mV (0.3 mV: $P = 0.034$, 0.4 mV: $P = 0.039$, 0.5 mV: $P = 0.025$, Supplementary Fig. 8B, middle panel). In the CA1 region, analysis of input-output strength revealed significant alterations between groups at fiber volley amplitudes between 0.4 and 0.8 mV (0.4 mV: $P = 0.032$, 0.5 mV: $P = 0.039$, 0.6 mV: $P = 0.006$, 0.7 mV: $P = 0.003$, 0.8 mV: $P = 0.011$, Supplementary Fig. 8 C, middle panel).

All together, these results show that CB1 deletion from proliferating cells in the dentate gyrus can result in alterations in LTP both within and outside the DG (MPP-DG and CA3-CA1).

Spatial memory and behavioral despair are regulated by CB1 in adult-born neurons

We next tested the animals in emotion- and memory-related hippocampus-dependent behavioral tasks, which have been implicated to be influenced by newly born neurons (Anacker and Hen 2017).

Mice were tested on 28 dptm (Fig. 7A), starting with the spatial object recognition test in a Y-maze. Here, nes-CB1ko/ko mice showed a significant decrease ($P = 0.038$) in the index of recognition (CB1wt/wt: 61.1 ± 2.1%, nes-CB1ko/ko: 52.9 ± 3.4%),

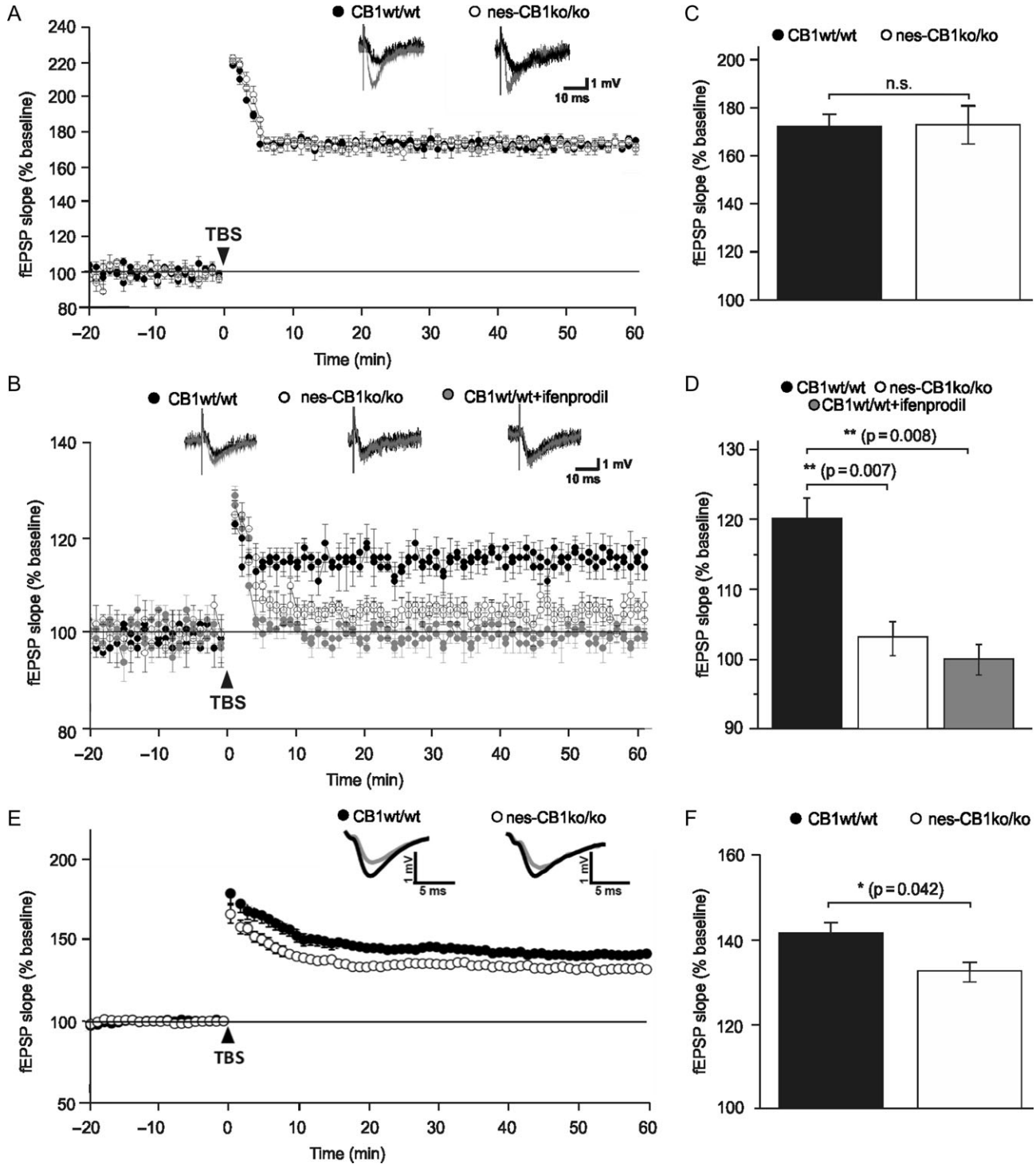

Figure 6. Summary plots of the field EPSP (fEPSP) slope elicited in response to a test stimulus before (-20 to 0 min) and after (0 to 60 min) tetanic stimulation of the medial perforant path (MPP) in (A) nes-CB1ko/ko (n = 8 slices, two animals) and in CB1wt/wt (n = 9 slices, three animals) in presence of picrotoxin, 28 to 42 dptm, and (B) in nes-CB1ko/ko (n = 12 slices, four animals) and in CB1wt/wt in absence (n = 11 slices, four animals) or presence (n = 8 slices, three animals) of ifenprodil, 28 to 42 dptm. (C, D) Averaged potentiation levels during the last 5 minutes of LTP in the conditions depicted in A and B respectively. **P < 0.01, one-way ANOVA. (E) fEPSPs were recorded in CA1 region by stimulating Schaffer collateral axons of area CA3. Acute slices of nes-CB1ko/ko mice (n = 16 slices, four animals) displayed an LTP curve that is significantly different to that of littermate controls (n = 23 slices, five animals). (F) Averaged potentiation levels during the last 5 minutes of LTP are significantly lower in nes-CB1ko/ko than in CB1wt/wt mice, *P < 0.05, two-tailed unpaired Student's t-test, t = 2.102. Data are represented as mean ± SEM.

while total exploration time and distance moved were unaltered (Fig. 7B). The reduced index of recognition implies that deletion of CB1 from NSCs deteriorates cognitive performance. When testing animals in the Morris water maze (MWM) test, both groups were equally able to find the visible platform. During training with the hidden platform, nes-CB1ko/ko mice

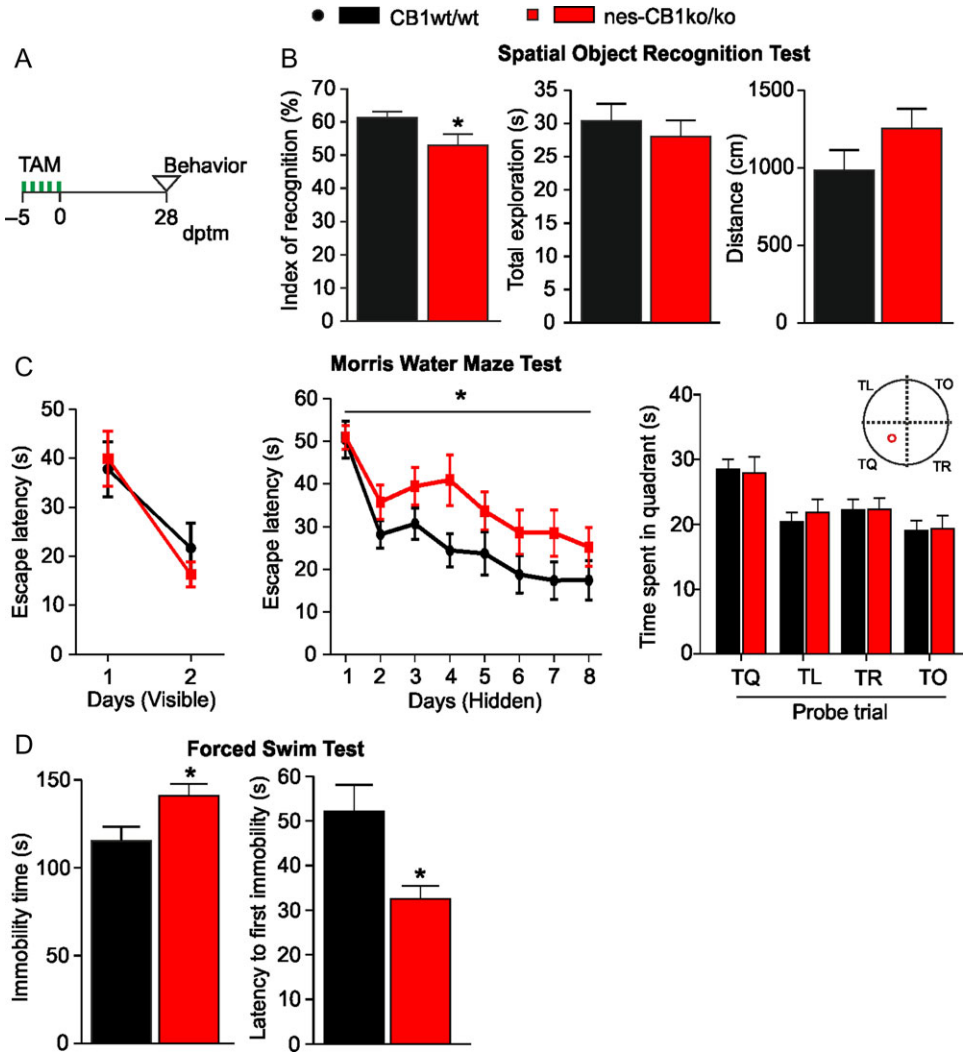

Figure 7. (A) Behavior of CB1wt/wt and nes-CB1ko/ko mice was analyzed at 28 dptm. (B) nes-CB1ko/ko mice in the spatial object recognition test displayed a decrease in the index of recognition, whereas total exploration and total distance traveled were not impaired. $N = 19$ (CB1wt/wt), $n = 13$ (nes-CB1ko/ko), $^*P < 0.05$, two-tailed unpaired Student's t-test. (C) Animals in the Morris water maze test exhibited no genotype difference in escape latency during visible platform trainings. Nes-CB1ko/ko mice showed a decreased performance in Morris water maze training during the days hidden platform search; $n = 20$ (CB1wt/wt), $n = 19$ (nes-CB1ko/ko), $^*P < 0.05$, repeated measure 2-way ANOVA; Bonferroni post-test, $F = 4.74$. After 8 days of training, both genotypes spent the same time in the target quadrant (TQ) during the probe trial. TR, target right; TO, target opposite; TL, target left. (D) nes-CB1ko/ko mice displayed an increase in immobility time and a decrease in latency to first immobility in the forced swim test. $N = 19$ (CB1wt/wt), $n = 13$ (nes-CB1ko/ko), $^*P < 0.05$, two-tailed unpaired Student's t-test. Graphs show mean ± SEM.

displayed higher escape latencies ($P = 0.036$) over the time course of 8 days, indicating that CB1 deletion leads to impaired learning acquisition of spatial cues. However, during the probe trial, all animals spent the same amount of time in the target quadrant (CB1wt/wt: 28.5 ± 1.5 s, nes-CB1ko/ko: 27.9 ± 2.4 s), suggesting that finally the spatial engram was memorized the same in the two genotypes (Fig. 7C).

As it is known that the process of adult neurogenesis regulates behavioral despair, animals were analyzed in the forced swim test, which has been used as a test to assess depressive-like behavior or efficacy of antidepressant drugs. Animals lacking CB1 displayed an increase ($P = 0.031$) in immobility time (nes-CB1ko/ko: 141.0 ± 6.7 s; CB1wt/wt: 115.2 ± 8.2 s) and a decrease ($P = 0.017$) in latency to first immobility (nes-CB1ko/ko: 32.5 ± 2.9 s; CB1wt/wt: 52.1 ± 6.0 s) (Fig. 7D). In contrast, CB1 deletion did not affect body weight, locomotion, nor anxiety-like behavior in the open field and light dark test (Supplementary Fig. 9A-C).

In conclusion, CB1-induced impairments on the cellular level led to a significant deterioration in spatial learning and memory, as well as to an enhancement of behavioral despair.

Discussion

A central question in the field of adult neurogenesis is how the multitude of signals in the neurogenic niche regulates NSC fate. It has been known that endocannabinoids regulate adult neurogenesis as part of the niche signals, by acting in an autocrine and/or paracrine fashion on the cannabinoid receptors CB1 and CB2 (Prenderville et al. 2015). However, it has remained elusive, whether cannabinoid receptor signaling acts directly via its expression in NSCs and its progeny (Aguado et al. 2006; Palazuelos et al. 2006) or whether receptor signaling works indirectly via niche-surrounding cells, which by themselves produce signaling molecules or alter neurotransmitter release. The present study addressed the regulation of adult neurogenesis

by studying the direct function of NSC lineage-specific CB1 in the adult mouse dentate gyrus *in vivo*. To this end, we developed a transgenic strategy to conditionally inactivate CB1 in adult NSCs and their progeny, and investigated the direct role of CB1 on adult neurogenesis, electrophysiological properties of newborn neurons, and neurogenesis-related behavior.

Selective deletion of CB1 from nestin-positive cells led to a decrease in total adult-born cells in the DG, caused by a reduction in NSC/NPC proliferation, without affecting apoptosis of newly generated cells. However, survival defects due to the caspase-independent form of programmed cell-death ferroptosis cannot be excluded. As the proliferation marker BrdU is predicted to interfere with the cell cycle and therefore could lead to changes in cellular fate (Duque and Rakic 2011), we backed up our observation using genetic labeling with YFP. The observed defect in proliferation was additionally supported by a second approach targeting Sox2-positive NSCs with a lentiviral vector. Our data demonstrate that the reduction in NSC/NPC proliferation, which was previously shown in complete CB1 knock-out animals (Aguado et al. 2006), is caused by the loss of CB1 expressed directly in NSCs and not in surrounding cells, e.g., glutamatergic Mossy cells and GABAergic interneurons in close proximity. Interestingly, the proliferation rate of recombined cells in the SVZ was unchanged between CB1wt/wt and nes-CB1ko/ko animals, which accounts for a region-specific effect of CB1 on NSC/NPC proliferation in the adult. Even if adult NSCs and progenitors in the DG and SVZ share some cellular characteristics reflected by the expression of common specific transcription factors, they are clearly of different embryonic origin (Fuentealba et al. 2015; Berg et al. 2018) and are equipped with distinct transcriptional profiles (Hsieh 2012). These features may explain that the regulative effect of CB1 on proliferation is exerted only in DG NSCs/NPCs. Additionally, differences in ligand availability in both neurogenic niches could account for the observed differences.

2-AG signaling was proposed to be functional in neural stem cells in an autocrine manner (Oudin, Hobbs, et al. 2011). Our data provide hints that 2-AG levels in the hippocampal neurogenic niche did not depend on CB1 expressed in NSC, as we detected no genotype differences in DAGLα mRNA levels in FACS-isolated $CD133^{+}$ neural stem cells. Thus, there appears no crosstalk between CB1 signaling and DAGLα expression. This implicates that CB1 is necessary for proper NSC/NPC proliferation, even in the presence functional 2-AG. On the other hand, 2-AG signaling is also indispensable, as other works showed deteriorated adult neurogenesis caused by reduced proliferation in DAGLα and DAGLβ knock-out mice (Gao et al. 2010) or by pharmacological blockade of DAGL (Goncalves et al. 2008).

The activation of CB1 via endocannabinoid signaling in NSCs/NPCs might involve the proliferative signal transduction pathways PI3K/Akt and ERK (Galve-Roperh et al. 2002), two classical pathways which promote cell survival and proliferation. Downstream targets, in turn, may include mTORC1 and CREB, which are central regulators of immediate early genes, such as c-fos, c-jun, zif268, and BDNF, leading to neural cell survival/death decisions (Prenderville et al. 2015) or NSC proliferation (Li et al. 2008). Indeed, we found a reduction of BDNF mRNA in DG neurospheres of animals lacking CB1 in NSCs/NPCs. Furthermore, we detected a downregulation of CB2. To our knowledge, there are no published data describing a direct regulation of CB1 on CB2 expression. However, other groups have shown an increase of adult NSC/NPC proliferation rate when using the selective CB2 agonist HU-308 (Palazuelos et al. 2006). Additionally, CB1 might interact with growth factors by transactivating e.g., the EGF receptor (Hart et al. 2004) or the major BDNF receptor TrkB (Berghuis et al. 2005). Even though proliferation was reduced, we did not detect a lineage switch in the differentiation potential of CB1-deficient NSCs. This points towards a non-cell autonomous effect of CB1 on differentiation when compared to the results of Aguado and colleagues (Aguado et al. 2006), who showed a deficit in hippocampal astrogliogenesis in complete CB1 knock-out mice. In that work, CB1 deletion on cells other than NSCs inside the niche may have indirectly increased neurogenesis or reduced astrogliogenesis; e.g., CB1 acting on glutamatergic or GABAergic neurons and on astrocytes. Regardless of an unchanged differentiation potential in our study, we detected a reduced number of astrocytes, neuroblasts and mature granule cells as a consequence of reduced proliferation at early stages of neurogenesis.

The observation that independent of the genotype, the pool of YFP-positive neurons increased from 28 dptm to 56 dptm whereas the population of YFP-positive astrocytes decreased, could be explained by the fact that the differentiated progeny derives from distinct NSC types. Neuronal cells are derived from fast dividing intermediate progenitors (type-2 cells), which increase the pool of initially recombined cells in a short amount of time. Furthermore, the development of mature NeuN-positive neurons approximately takes around two month (~56 days) (Zhao et al. 2008), explaining why the majority of NeuN-positive recombined cells is observed at 56 dptm. In contrast, astrocytes derive from more quiescent nestin-positive radial glia-like cells (type-1 cells) (Bonaguidi et al. 2011; Encinas et al. 2011; Berg et al. 2018), explaining why we did not detect an increase in recombined astrocytic cells four weeks after. A decrease instead could be explained by the fact that initially more type-2 than type-1 cells had recombined and that during tissue homeostasis dying astrocytes later were replenished from initially non-recombined cells. Furthermore, recombination in resident nestin re-expressing astrocytes cannot be excluded, which then also could be renewed from non-recombined progenitors.

Stereological counts revealed that 12 000–15 000 newly generated cells were targeted in wild-type mice (concordant with Lagace et al. 2007), representing 2.4–3% of the total DG granule cell population (500,000 cells (Ihunwo and Schliebs 2010)). Reduction of neurogenesis in nes-CB1ko/ko mice led to 8 000–11 000 cells, constituting only 1.6–2.2% of total cells. In electrophysiological experiments, NSC-specific CB1 deletion revealed an impairment of LTP in the DG and in pyramidal neurons of the CA1 region. The latter could be the result of circuit remodeling induced by potential changes of mossy fiber-LTP which might have induced structural changes/connectivity in CA3 and finally downstream changes in Schaffer-collateral LTP. Furthermore, we showed that loss of CB1 signaling led to a specific form of strongly impaired LTP in young neurons, comparable to LTP observed in ifenprodil-treated slices from CB1wt/wt mice. Glutamatergic signaling in mature granule neurons was not affected by CB1 deletion, as shown by experiments where GABAergic inhibition in the DG was blocked with picrotoxin. Our data are in concert with a study showing that blocked hippocampal neurogenesis by irradiation led to the same reduced ifenprodil-sensitive LTP at MPP-DG synapses (Snyder et al. 2001). However, in addition to the reduced number of newborn neurons, impaired LTP formation could also result from a reduced dendritic arborization pattern. Indeed, our data showed that CB1-deficient newborn neurons displayed a reduction in dendritic length and spine density, but had no defect in axonal growth, indicating that CB1 is required for proper dendritic maturation of adult-born neurons originating from NSCs in the SGZ. It has previously been

shown that CB1 has an impact on neuronal and synaptic maturation via regulating growth cone motility and neuritogenesis during embryonic development (Williams et al. 2003; Berghuis et al. 2007; Watson et al. 2008). Furthermore, autocrine and paracrine endocannabinoid-signaling regulates migration of SVZ-derived neuroblasts in the postnatal brain by CB1 and DAGLα, which are co-expressed in growth cones (Oudin, Gajendra, et al. 2011). As we detected no inhibition of axonal growth on newborn neurons devoid of CB1, our data support the possibility that axonal elongation of newborn hippocampal neurons is differently regulated as compared to neuroblast migration in the adult SVZ. DAGLα, which is required for axonal growth during development and for retrograde synaptic signaling at mature synapses with high dendritic expression levels, has been postulated to function as a "dendrite initiation factor" by postsynaptic production of 2-AG (Bisogno et al. 2003; Reisenberg et al. 2012). For this reason, we analyzed whether the impaired dendritic growth could be related to a decreased DAGLα expression in newborn neurons, caused by the lack of CB1 signaling. However, we found that deterioration of dendritic growth was 2-AG-independent, as DAGLα expression was not altered in FACS-isolated PSA-NCAM$^+$ newborn neurons and CD133$^+$ stem cells isolated from wildtype and NSC-specific CB1 knock-out mice. The data pinpoint again to a clear necessity of CB1 in proper dendritic growth, despite unaltered availability of 2-AG. Interestingly, DAGLα mRNA was significantly increased in developing newborn neurons compared to stem cells. These data fit with work from Jung et al. (2011), showing an increase of DAGL during RA-induced differentiation of Neuro2A cells. However, our results are in conflict with observations on differentiating the neural stem cell line Cor-1 (Walker et al. 2010). The difference could be explained by the fact that the latter cell line gives rise to GABAergic interneurons, which in their mature state do not express DAGLα anymore (Berghuis et al. 2007), but mature DG granule neurons originating from newborn hippocampal PSA-NCAM$^+$ cells do (Sugaya et al. 2016).

In addition to the predominantly presynaptic expression of CB1, postsynaptic localization has also been demonstrated (Njoo et al. 2015; Maroso et al. 2016). Even if we have not tested whether maturing granule neurons display postsynaptic CB1, this scenario could likely account for the dendritic defects seen in the progeny of CB1-deficient NSCs. Alternatively, earlier signaling events at the level of NSCs or neuroblasts may already determine dendritic length. Signaling cascades could involve BDNF as a potent regulator of dendritic outgrowth (Tolwani et al. 2002), which has been shown to act via autocrine signaling in adult born granule cells (Wang et al. 2015). However, BDNF also positively regulates dendritic arbor complexity, which was not affected in our study. It is known that distinct molecules regulate outgrowth and branching (Jan and Jan 2010). For this reason, direct CB1 signaling in neuroblasts or maturing granule neurons could trigger gene expression of only outgrowth-related proteins.

In addition to reduced LTP at the MPP-DG synapses, we also found a small but significant decrease of LTP even in the CA1 field in the mutant mice, revealing functional alterations beyond the CB1-deficiency in the MPP-DG path. These results indicate that the ability of the DG to continuously add new granule cells may exert surprisingly long-range effects on downstream circuits (Song et al. 2012).

A decrease in adult neurogenesis has been shown to influence cognitive performance and mood regulation (Fanselow and Dong 2010; Anacker and Hen 2017). When we tested nes-CB1ko/ko mice in neurogenesis-related behavioral paradigms, hippocampus-dependent spatial learning was affected and depressive-like behavior was induced. Nes-CB1ko/ko mice exhibited a marked decrease in spatial learning in the Morris water maze, which is consistent with data from other studies where the number of newborn cells was reduced (Goncalves et al. 2016). Furthermore, we showed that nes-CB1ko/ko mice exhibit deterioration of cognitive performance and of innate preference for novelty in another hippocampus-dependent test, the spatial object recognition test. This test requires the hippocampus for encoding, consolidation, and retrieval, and assesses short-term spatial memory in the mouse. Our results are in accordance with another study addressing adult neurogenesis and cognition, which showed that the amount of neuroblasts was positively correlated to the reaction to novelty (van Dijk et al. 2016). Functional studies and computational modeling of the effects of adult neurogenesis on hippocampal function have generated different theories for the role of newborn neurons (Goncalves et al. 2016). These include the formation of temporal and spatial associations in memory (Aimone et al. 2006; Becker and Wojtowicz 2007) and cognitive flexibility during learning of new tasks (Chambers et al. 2004) as well as balancing pattern separation/integration (Aimone et al. 2009). Furthermore, functional adult neurogenesis has been implicated in the pathophysiology of major depression. A significant subpopulation of patients with major depression was shown to have a reduced hippocampal volume potentially due to decreased neurogenesis, and these patients displayed cognitive deficits (Goncalves et al. 2016). In addition, antidepressant treatment leads to clinical improvement associated with a slow, temporal increase in adult hippocampal neurogenesis (Miller and Hen 2015). However, more data are needed to determine whether a neurogenic decline is causative or associative with the occurrence of major depression. In the present study, nes-CB1ko/ko mice displayed an increase in behavioral despair in the forced swim test. Presumably, the pattern of hypoproliferation in nes-CB1-deficient mice in this study is similar to alterations in neurogenesis during depression, suggesting that a neurogenic failure could lead to depressive-like behavior.

Altogether, our data underline the importance of functional neurogenesis in the adult mouse DG, which serves as a major input region to the hippocampus and, therefore, is thought to play a key role in learning, memory and spatial navigation tasks. Furthermore, our data indicate the necessity of functional adult neurogenesis to serve as a reservoir for stress resilience and vulnerability in neuropsychiatric disorders (Levone et al. 2015). Here, we showed that ablating intrinsic signaling of NSC-resident CB1 is sufficient to lead to detrimental effects at the structural, physiological and behavioral level in adult mice.

Supplementary Material

Supplementary material is available at *Cerebral Cortex* online.

Funding

This work was supported partially by the German Research Foundation (CRC 1193, project A02 to Benedikt Berninger and Beat Lutz). Cell Sorting experiments were funded by the Boehringer Ingelheim Foundation (to Beat Lutz). The electrophysiological experiments were partially funded by the U.S. National Institutes of Health (NS99457) to Ivan Soltesz.

Notes

We thank Günther Schütz for providing us with the Nestin-CreERT2 mouse line. We thank Guillerme Horta and Konstantin

Radyushkin for help with analysis of the Morris Water Maze test. In addition, we thank Andrea Conrad, Ruth Jelinek, Marcus Keil and Christina Maul for excellent technical assistance. We thank the viral vector facility of the CRC 1080 funded by the DFG (German Research Foundation) for retroviral vector production, and Hoonkyo Suh for providing with the lentiviral vector Sox2-GFP/CRE. In addition, we thank the Institute of Molecular Biology (IMB, Mainz, Germany) Core Facilities Microscopy and Flow Cytometry for their contributions and valuable services. *Conflict of Interest*: None declared.

References

Aguado T, Monory K, Palazuelos J, Stella N, Cravatt B, Lutz B, Marsicano G, Kokaia Z, Guzman M, Galve-Roperh I. 2005. The endocannabinoid system drives neural progenitor proliferation. FASEB J. 19:1704–1706.

Aguado T, Palazuelos J, Monory K, Stella N, Cravatt B, Lutz B, Marsicano G, Kokaia Z, Guzman M, Galve-Roperh I. 2006. The endocannabinoid system promotes astroglial differentiation by acting on neural progenitor cells. J Neurosci. 26: 1551–1561.

Aimone JB, Li Y, Lee SW, Clemenson GD, Deng W, Gage FH. 2014. Regulation and function of adult neurogenesis: from genes to cognition. Physiol Rev. 94:991–1026.

Aimone JB, Wiles J, Gage FH. 2006. Potential role for adult neurogenesis in the encoding of time in new memories. Nat Neurosci. 9:723–727.

Aimone JB, Wiles J, Gage FH. 2009. Computational influence of adult neurogenesis on memory encoding. Neuron. 61: 187–202.

Anacker C, Hen R. 2017. Adult hippocampal neurogenesis and cognitive flexibility - linking memory and mood. Nat Rev Neurosci. 18:335–346.

Araque A, Castillo PE, Manzoni OJ, Tonini R. 2017. Synaptic functions of endocannabinoid signaling in health and disease. Neuropharmacology. 124:13–24.

Becker S, Wojtowicz JM. 2007. A model of hippocampal neurogenesis in memory and mood disorders. Trends Cogn Sci. 11:70–76.

Berg D, Bond AM, Ming G, Song H. 2018. Radial glial cells in the adult dentate gyrus: what are they and where do they come from? F1000Res. 7:277.

Bergami M, Rimondini R, Santi S, Blum R, Götz M, Canossa M. 2008. Deletion of TrkB in adult progenitors alters newborn neuron integration into hippocampal circuits and increases anxiety-like behavior. Proc Natl Acad Sci USA. 105: 15570–15575.

Berghuis P, Dobszay MB, Wang X, Spano S, Ledda F, Sousa KM, Schulte G, Ernfors P, Mackie K, Paratcha G, et al. 2005. Endocannabinoids regulate interneuron migration and morphogenesis by transactivating the TrkB receptor. Proc Natl Acad Sci USA. 102:19115–19120.

Berghuis P, Rajnicek AM, Morozov YM, Ross RA, Mulder J, Urban GM, Monory K, Marsicano G, Matteoli M, Canty A, et al. 2007. Hardwiring the brain: endocannabinoids shape neuronal connectivity. Science. 316:1212–1216.

Bertrand N, Castro DS, Guillemot F. 2002. Proneural genes and the specification of neural cell types. Nat Rev Neurosci. 3: 517–530.

Bisogno T, Howell F, Williams G, Minassi A, Cascio MG, Ligresti A, Matias I, Schiano-Moriello A, Paul P, Williams EJ, et al. 2003. Cloning of the first sn1-DAG lipases points to the spatial and temporal regulation of endocannabinoid signaling in the brain. J Cell Biol. 163:463–468.

Boldrini M, Fulmore CA, Tartt AN, Simeon LR, Pavlova I, Poposka V, Rosoklija GB, Stankov A, Arango V, Dwork AJ, et al. 2018. Human Hippocampal Neurogenesis Persists throughout Aging. Cell Stem Cell. 22:589–599.

Bonaguidi MA, Wheeler MA, Shapiro JS, Stadel RP, Sun GJ, Ming G, Song H. 2011. In vivo clonal analysis reveals self-renewing and multipotent adult neural stem cell characteristics. Cell. 145:1142–1155.

Bond AM, Ming GL, Song H. 2015. Adult mammalian neural stem cells and neurogenesis: five decades later. Cell Stem Cell. 17:385–395.

Campos AC, Ortega Z, Palazuelos J, Fogaca MV, Aguiar DC, Diaz-Alonso J, Ortega-Gutiérrez S, Vázquez-Villa H, Moreira FA, Guzmán M, et al. 2013. The anxiolytic effect of cannabidiol on chronically stressed mice depends on hippocampal neurogenesis: involvement of the endocannabinoid system. Int J Neuropsychopharmacol. 16:1407–1419.

Chambers RA, Potenza MN, Hoffman RE, Miranker W. 2004. Simulated apoptosis/neurogenesis regulates learning and memory capabilities of adaptive neural networks. Neuropsychopharmacology. 29:747–758.

Cipriani S, Ferrer I, Aronica E, Kovacs GG, Verney C, Nardelli J, Khung S, Delezoide AL, Milenkovic I, Rasika S, et al. 2018. Hippocampal Radial Glial Subtypes and Their Neurogenic Potential in Human Fetuses and Healthy and Alzheimer's Disease Adults. Cereb Cortex. 28:2458–2478.

Corsini NS, Sancho-Martinez I, Laudenklos S, Glagow D, Kumar S, Letellier E, Koch P, Teodorczyk M, Kleber S, Klussmann S, et al. 2009. The death receptor CD95 activates adult neural stem cells for working memory formation and brain repair. Cell Stem Cell. 5:178–190.

Danielson NB, Kaifosh P, Zaremba JD, Lovett-Barron M, Tsai J, Denny CA, Balough EM, Goldberg AR, Drew LJ, Hen R, et al. 2016. Distinct contribution of adult-born hippocampal granule cells to context encoding. Neuron. 90:101–112.

Dennis CV, Suh LS, Rodriguez ML, Kril JJ, Sutherland GT. 2016. Human adult neurogenesis across the ages: An immunohistochemical study. Neuropathol Appl Neurobiol. 42:621–638.

Deshpande A, Bergami M, Ghanem A, Conzelmann KK, Lepier A, Götz M, Berninger B. 2013. Retrograde monosynaptic tracing reveals the temporal evolution of inputs onto new neurons in the adult dentate gyrus and olfactory bulb. Proc Natl Acad Sci U S A. 110:E1152–E1161.

Dubreucq S, Koehl M, Abrous DN, Marsicano G, Chaouloff F. 2010. CB1 receptor deficiency decreases wheel-running activity: consequences on emotional behaviours and hippocampal neurogenesis. Exp Neurol. 224:106–113.

Dupret D, Fabre A, Döbrössy MD, Panatier A, Rodríguez JJ, Lamarque S, Lemaire V, Oliet SH, Piazza PV, Abrous DN. 2007. Spatial learning depends on both the addition and removal of new hippocampal neurons. PLoS Biol. 5:e214.

Duque A, Rakic P. 2011. Different effects of bromodeoxyuridine and [3H]thymidine incorporation into DNA on cell proliferation, position, and fate. J Neurosci. 31:15205–15217.

Díaz-Alonso J, de Salas-Quiroga A, Paraíso-Luna J, García-Rincón D, Garcez PP, Parsons M, Andradas C, Sánchez C, Guillemot F, Guzmán M, et al. 2017. Loss of cannabinoid CB1 receptors induces cortical migration malformations and increases seizure susceptibility. Cereb Cortex. 27: 5303–5317.

D'Souza DC, Pittman B, Perry E, Simen A. 2009. Preliminary evidence of cannabinoid effects on brain-derived neurotrophic

factor (BDNF) levels in humans. Psychopharmacology (Berl). 202:569–578.

Encinas JM, Michurina TV, Peunova N, Park JH, Tordo J, Peterson DA, Fishell G, Koulakov A, Enikolopov G. 2011. Division-coupled astrocytic differentiation and age-related depletion of neural stem cells in the adult hippocampus. Cell Stem Cell. 8:566–579.

Fanselow MS, Dong HW. 2010. Are the dorsal and ventral hippocampus functionally distinct structures? Neuron. 65:7–19.

Fuentealba LC, Rompani SB, Parraguez JI, Obernier K, Romero R, Cepko CL, Alvarez-Buylla A. 2015. Embryonic origin of postnatal neural stem cells. Cell. 161:1644–1655.

Galve-Roperh I, Aguado T, Palazuelos J, Guzman M. 2007. The endocannabinoid system and neurogenesis in health and disease. Neuroscientist. 13:109–114.

Galve-Roperh I, Aguado T, Palazuelos J, Guzman M. 2008. Mechanisms of control of neuron survival by the endocannabinoid system. Curr Pharm Des. 14:2279–2288.

Galve-Roperh I, Rueda D, Gomez del PT, Velasco G, Guzman M. 2002. Mechanism of extracellular signal-regulated kinase activation by the CB(1) cannabinoid receptor. Mol Pharmacol. 62:1385–1392.

Gao Y, Vasilyev DV, Goncalves MB, Howell FV, Hobbs C, Reisenberg M, Shen R, Zhang MY, Strassle BW, Lu P, et al. 2010. Loss of retrograde endocannabinoid signaling and reduced adult neurogenesis in diacylglycerol lipase knockout mice. J Neurosci. 30:2017–2024.

Goncalves JT, Schafer ST, Gage FH. 2016. Adult Neurogenesis in the hippocampus: from stem cells to behavior. Cell. 167: 897–914.

Goncalves MB, Suetterlin P, Yip P, Molina-Holgado F, Walker DJ, Oudin MJ, Zentar MP, Pollard S, Yáñez-Muñoz RJ, Williams G, et al. 2008. A diacylglycerol lipase-CB2 cannabinoid pathway regulates adult subventricular zone neurogenesis in an age-dependent manner. Mol Cell Neurosci. 38:526–536.

Gowran A, Noonan J, Campbell VA. 2011. The multiplicity of action of cannabinoids: implications for treating neurodegeneration. CNS Neurosci Ther. 17:637–644.

Hart S, Fischer OM, Ullrich A. 2004. Cannabinoids induce cancer cell proliferation via tumor necrosis factor alpha-converting enzyme (TACE/ADAM17)-mediated transactivation of the epidermal growth factor receptor. Cancer Res. 64:1943–1950.

Hsieh J. 2012. Orchestrating transcriptional control of adult neurogenesis. Genes Dev. 26:1010–1021.

Ihunwo AO, Schliebs R. 2010. Cell proliferation and total granule cell number in dentate gyrus of transgenic Tg2576 mouse. Acta Neurobiol Exp (Wars). 70:362–369.

Jan YN, Jan LY. 2010. Branching out: mechanisms of dendritic arborization. Nat Rev Neurosci. 11:316–328.

Jiang W, Zhang Y, Xiao L, Van Cleemput J, Ji SP, Bai G, Zhang X. 2005. Cannabinoids promote embryonic and adult hippocampus neurogenesis and produce anxiolytic- and antidepressant-like effects. J Clin Invest. 115:3104–3116.

Jin K, Xie L, Kim SH. 2004. Defective adult neurogenesis in CB1 cannabinoid receptor knockout mice. Mol Pharmacol. 66: 204–208.

Jung KM, Astarita G, Thongkham D, Piomelli D. 2011. Diacylglycerol lipase-alpha and -beta control neurite outgrowth in neuro-2a cells through distinct molecular mechanisms. Mol Pharmacol. 80:60–67.

Kempermann G. 2011. Adult neurogenesis. vol. 2. Oxford: Oxford University Press. p. 378–388.

Kempermann G, Gage FH, Aigner L, Song H, Curtis MA, Thuret S, Kuhn HG, Jessberger S, Frankland PW, Cameron HA, et al. 2018. Human Adult Neurogenesis: Evidence and Remaining Questions. Cell Stem Cell. 23:25–30.

Kendall DA, Yudowski GA. 2017. Cannabinoid receptors in the central nervous system: their signaling and roles in disease. Front Cell Neurosci. 10:294. doi:10.3389/fncel.2016.00294.

Lagace DC, Whitman MC, Noonan MA, Ables JL, DeCarolis NA, Arguello AA, Donovan MH, Fischer SJ, Farnbauch LA, Beech RD, et al. 2007. Dynamic contribution of nestin-expressing stem cells to adult neurogenesis. J Neurosci. 27:12623–12629.

Levone BR, Cryan JF, O'Leary OF. 2015. Role of adult hippocampal neurogenesis in stress resilience. Neurobiol Stress. 1: 147–155.

Li Y, Luikart BW, Birnbaum S, Chen J, Kwon CH, Kernie SG, Bassel-Duby R, Parada LF. 2008. TrkB regulates hippocampal neurogenesis and governs sensitivity to antidepressive treatment. Neuron. 59:399–412.

Marchalant Y, Brothers HM, Wenk GL. 2009. Cannabinoid agonist WIN-55,212-2 partially restores neurogenesis in the aged rat brain. Mol Psychiatry. 14:1068–1069.

Maroso M, Szabo GG, Kim HK, Alexander A, Bui AD, Lee SH, Lutz B, Soltesz I. 2016. Cannabinoid control of learning and memory through HCN channels. Neuron. 89:1059–1073.

Marsicano G, Goodenough S, Monory K, Hermann H, Eder M, Cannich A, Azad SC, Cascio MG, Gutierrez SO, van der Stelt M, et al. 2003. CB1 cannabinoid receptors and on-demand defense against excitotoxicity. Science. 302:84–88.

Marsicano G, Kuner R. 2008. Anatomical distribution of receptors, ligands and enzymes in the brain and in the spinal cord: circuitries and neurochemistry. In: A Köfalvi , editor. Cannabinoids and the brain. Boston: Springer US. p. 161–201.

Miller BR, Hen R. 2015. The current state of the neurogenic theory of depression and anxiety. Curr Opin Neurobiol. 30: 51–58.

Monory K, Massa F, Egertova M, Eder M, Blaudzun H, Westenbroek R, Kelsch W, Jacob W, Marsch R, Ekker M, et al. 2006. The endocannabinoid system controls key epileptogenic circuits in the hippocampus. Neuron. 51:455–466.

Mu Y, Lee SW, Gage FH. 2010. Signaling in adult neurogenesis. Curr Opin Neurobiol. 20:416–423.

Mulder J, Aguado T, Keimpema E, Barabas K, Ballester Rosado CJ, Nguyen L, Monory K, Marsicano G, Di Marzo V, Hurd YL, et al. 2008. Endocannabinoid signaling controls pyramidal cell specification and long-range axon patterning. Proc Natl Acad Sci U S A. 105:8760–8765.

Njoo C, Agarwal N, Lutz B, Kuner R. 2015. The cannabinoid receptor CB1 interacts with the WAVE1 complex and plays a role in actin dynamics and structural plasticity in neurons. PLoS Biol. 13:e1002286.

Oudin MJ, Gajendra S, Williams G, Hobbs C, Lalli G, Doherty P. 2011. Endocannabinoids regulate the migration of subventricular zone-derived neuroblasts in the postnatal brain. J Neurosci. 31:4000–4011.

Oudin MJ, Hobbs C, Doherty P. 2011. DAGL-dependent endocannabinoid signalling: roles in axonal pathfinding, synaptic plasticity and adult neurogenesis. Eur J Neurosci. 34: 1634–1646.

Pagotto U, Marsicano G, Cota D, Lutz B, Pasquali R. 2006. The emerging role of the endocannabinoid system in endocrine regulation and energy balance. Endocr Rev. 27:73–100.

Palazuelos J, Aguado T, Egia A, Mechoulam R, Guzman M, Galve-Roperh I. 2006. Non-psychoactive CB2 cannabinoid agonists stimulate neural progenitor proliferation. FASEB J. 20:2405–2407.

Patzke N, Spocter MA, Karlsson KÆ, Bertelsen MF, Haagensen M, Chawana R, Streicher S, Kaswera C, Gilissen E, Alagaili AN, et al. 2015. In contrast to many other mammals, cetaceans have relatively small hippocampi that appear to lack adult neurogenesis. Brain Struct Funct. 220:361–383.

Pilz GA, Bottes S, Betizeau M, Jörg DJ, Carta S, Simons BD, Helmchen F, Jessberger S. 2018. Live imaging of neurogenesis in the adult mouse hippocampus. Science. 359:658–662.

Prenderville JA, Kelly AM, Downer EJ. 2015. The role of cannabinoids in adult neurogenesis. Br J Pharmacol. 172:3950–3963.

Reisenberg M, Singh PK, Williams G, Doherty P. 2012. The diacylglycerol lipases: structure, regulation and roles in and beyond endocannabinoid signalling. Philos Trans R Soc Lond B Biol Sci. 367:3264–3275.

Snyder JS, Kee N, Wojtowicz JM. 2001. Effects of adult neurogenesis on synaptic plasticity in the rat dentate gyrus. J Neurophysiol. 85:2423–2431.

Song J, Christian KM, Ming GL, Song H. 2012. Modification of hippocampal circuitry by adult neurogenesis. Dev Neurobiol. 72:1032–1043.

Song J, Sun J, Moss J, Wen Z, Sun GJ, Hsu D, Zhong C, Davoudi H, Christian KM, Toni N, et al. 2013. Parvalbumin interneurons mediate neuronal circuitry-neurogenesis coupling in the adult hippocampus. Nat Neurosci. 16:1728–1730.

Sorrells SF, Paredes MF, Cebrian-Silla A, Sandoval K, Qi D, Kelley KW, James D, Mayer S, Chang J, Auguste KI, et al. 2018. Human hippocampal neurogenesis drops sharply in children to undetectable levels in adults. Nature. 555:377–381.

Srinivas S, Watanabe T, Lin CS, William CM, Tanabe Y, Jessell TM, Costantini F. 2001. Cre reporter strains produced by targeted insertion of EYFP and ECFP into the ROSA26 locus. BMC Dev Biol. 1:4.

Sugaya Y, Yamazaki M, Uchigashima M, Kobayashi K, Watanabe M, Sakimura K, Kano M. 2016. Crucial roles of the endocannabinoid 2-arachidonoylglycerol in the suppression of epileptic seizures. Cell Rep. 16:1405–1415.

Suh H, Consiglio A, Ray J, Sawai T, D'Amour KA, Gage FH. 2007. In vivo fate analysis reveals the multipotent and self-renewal capacities of Sox2+ neural stem cells in the adult hippocampus. Cell Stem Cell. 1:515–528.

Temple S. 2001. The development of neural stem cells. Nature. 414:112–117.

Toda T, Gage FH. 2018. Review: adult neurogenesis contributes to hippocampal plasticity. Cell Tissue Res. 373:693–709. doi:10.1007/s00441-017-2735-4.

Toda T, Parylak SL, Linker SB, Gage FH. 2018. The role of adult hippocampal neurogenesis in brain health and disease. Mol Psychiatry. doi:10.1038/s41380-018-0036-2.

Tolwani RJ, Buckmaster PS, Varma S, Cosgaya JM, Wu Y, Suri C, Shooter EM. 2002. BDNF overexpression increases dendrite complexity in hippocampal dentate gyrus. Neuroscience. 114:795–805.

Toni N, Schinder AF. 2015. Maturation and functional integration of new granule cells into the adult hippocampus. Cold Spring Harb Perspect Biol. 8:a018903. doi:10.1101/cshperspect.a018903.

van Dijk RM, Lazic SE, Slomianka L, Wolfer DP, Amrein I. 2016. Large-scale phenotyping links adult hippocampal neurogenesis to the reaction to novelty. Hippocampus. 26:646–657.

Walker DJ, Suetterlin P, Reisenberg M, Williams G, Doherty P. 2010. Down-regulation of diacylglycerol lipase-alpha during neural stem cell differentiation: identification of elements that regulate transcription. J Neurosci Res. 88:735–745.

Wang L, Chang X, She L, Xu D, Huang W, Poo MM. 2015. Autocrine action of BDNF on dendrite development of adult-born hippocampal neurons. J Neurosci. 35:8384–8393.

Watson S, Chambers D, Hobbs C, Doherty P, Graham A. 2008. The endocannabinoid receptor, CB1, is required for normal axonal growth and fasciculation. Mol Cell Neurosci. 38:89–97.

Williams EJ, Walsh FS, Doherty P. 2003. The FGF receptor uses the endocannabinoid signaling system to couple to an axonal growth response. J Cell Biol. 160:481–486.

Wolf SA, Bick-Sander A, Fabel K, Leal-Galicia P, Tauber S, Ramirez-Rodriguez G, Müller A, Melnik A, Waltinger TP, Ullrich O, et al. 2010. Cannabinoid receptor CB1 mediates baseline and activity-induced survival of new neurons in adult hippocampal neurogenesis. Cell Commun Signal. 8:12.

Zhao C, Deng W, Gage FH. 2008. Mechanisms and functional implications of adult neurogenesis. Cell. 132:645–660.

Zhao M, Li D, Shimazu K, Zhou YX, Lu B, Deng CX. 2007. Fibroblast growth factor receptor-1 is required for long-term potentiation, memory consolidation, and neurogenesis. Biol Psychiatry. 62:381–390.

Zhao C, Teng EM, Summers RG Jr, Ming GL, Gage FH. 2006. Distinct morphological stages of dentate granule neuron maturation in the adult mouse hippocampus. J Neurosci. 26:3–11.